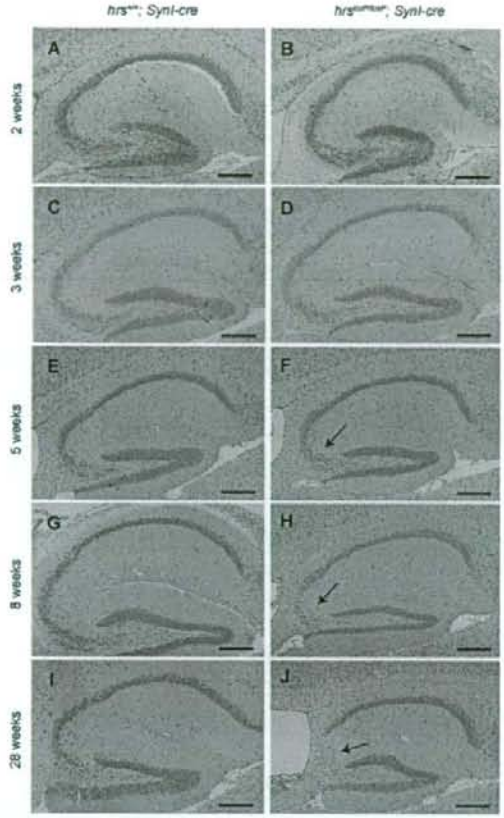

Figure 4. Abnormalities in the hippocampal CA3 subfield of *hrs*$^{loxP/loxP}$;*Synl-cre* mice. Nissl staining of anterior coronal hippocampus sections of mice. Mice were *hrs*$^{+/+}$;*Synl-cre* (**A**, **C**, **E**, **G**, **I**) and *hrs*$^{loxP/loxP}$;*Synl-cre* (**B**, **D**, **F**, **H**, **J**) and were 2 weeks (**A**, **B**), 3 weeks (**C**, **D**), 5 weeks (**E**, **F**), 8 weeks (**G**, **H**), and 28 weeks (**I**, **J**) of age. Note the loss of pyramidal cells in the CA3 subfield in the *hrs*$^{loxP/loxP}$;*Synl-cre* hippocampus (**arrows**). Scale bars = 250 μm. Original magnifications, ×100.

To examine the mossy fiber pathway that connects granule cells to CA3 pyramidal cells, we performed immunostaining assays for calbindin, which selectively stains neurons in the dentate gyrus containing the mossy fiber pathway and Purkinje cells. Despite the profound reduction of pyramidal cells in the hippocampal CA3 subfield of *hrs*$^{loxP/loxP}$;*Synl-cre* mice, the staining pattern of calbindin was not significantly different between the *hrs*$^{+/+}$;*Synl-cre* and *hrs*$^{loxP/loxP}$;*Synl-cre* mice (Figure 6, A and B). Immunohistochemical staining with an anti-calbindin antibody demonstrated no difference in the Purkinje cell numbers between the *hrs*$^{+/+}$;*Synl-cre* and *hrs*$^{loxP/loxP}$;*Synl-cre* mice (Figure 6, C and D).

Accumulation of Ubiquitinated Proteins in the Hrs Mutant Brain

Because Hrs has an essential role in the endocytic sorting of ubiquitinated proteins, we investigated whether

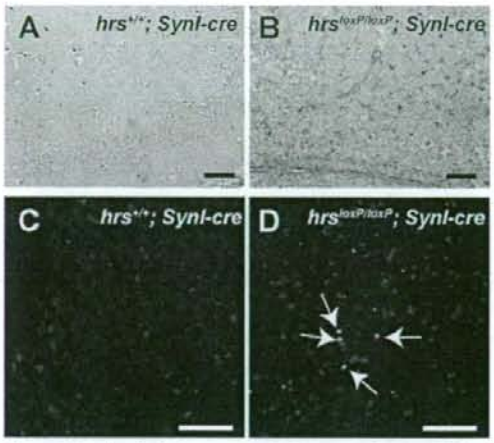

Figure 5. Neural cell death occurs in the hippocampal CA3 subfield of *hrs*$^{loxP/loxP}$;*Synl-cre* mice. **A** and **B:** Anti-GFAP antibody staining. Brain sections from *hrs*$^{+/+}$;*Synl-cre* (**A**) and *hrs*$^{loxP/loxP}$;*Synl-cre* (**B**) mice were immunostained with a GFAP-specific antibody. The GFAP signal was increased in the hippocampus of *hrs*$^{loxP/loxP}$;*Synl-cre* mice. **C** and **D:** TUNEL staining of the hippocampal CA3 subfield. Hippocampus sections of 5-week-old *hrs*$^{+/+}$;*Synl-cre* (**C**) and *hrs*$^{loxP/loxP}$;*Synl-cre* (**D**) mice were stained for TUNEL. **Arrows** indicate positive staining for TUNEL. Original magnifications, ×400. Scale bars = 50 μm.

ubiquitinated proteins accumulated in the Hrs mutant brains by immunohistochemical analysis. In the *hrs*$^{loxP/loxP}$;*Synl-cre* mouse brain, numerous granules stained by an anti-ubiquitin antibody appeared in the CA3 subfield, cerebral cortex, hypothalamus, and less frequently, in Purkinje cells (Figures 7 and 8). In the 16-week-old *hrs*$^{loxP/loxP}$;*Synl-cre* mouse brain, there were fewer ubiquitin-positive pyramidal cells, because most of the pyramidal cells were already lost (Figure 7, K–M). Interestingly, ubiquitin-positive aggregates were also observed in the 3-week-old *hrs*$^{loxP/loxP}$;*Synl-cre* mouse brain, which

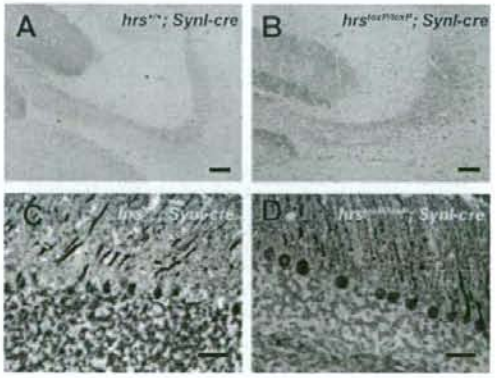

Figure 6. A and **B:** Calbindin immunostaining for mossy fibers. Sections were prepared from the brains of 8-week-old *hrs*$^{+/+}$;*Synl-cre* (**A**) and *hrs*$^{loxP/loxP}$;*Synl-cre* (**B**) mice. **C** and **D:** Calbindin immunostaining for Purkinje cells. The sections were prepared from the brains of 8-week-old *hrs*$^{+/+}$;*Synl-cre* (**C**) and *hrs*$^{loxP/loxP}$;*Synl-cre* (**D**) mice. Scale bars: 0.25 mm (**A**, **B**); 25 μm (**C**, **D**). Original magnifications: ×200 (**A**, **B**); ×400 (**C**, **D**).

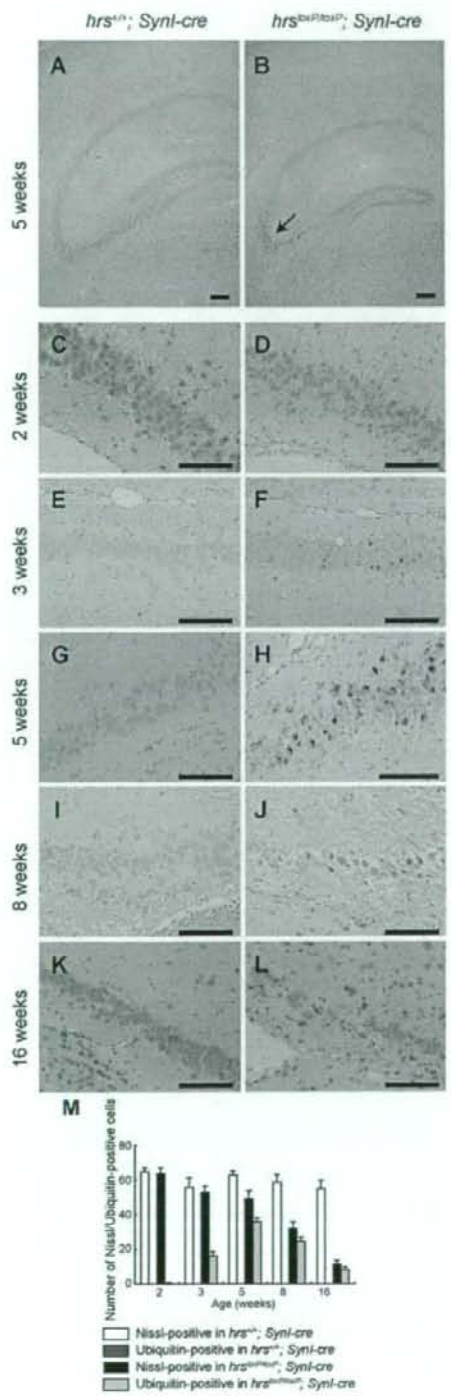

did not show the loss of hippocampal CA3 pyramidal neurons (Figure 4, C and D; and Figure 7, E, F, and M). The number of ubiquitin-positive neurons in the cerebral cortex gradually increased with age (Figure 8, A–J and O). On the other hand, we could not detect any ubiquitin-positive aggregates in the *hrs*$^{loxP/loxP}$*;MX1-cre* mouse liver, which was sufficiently knocked-out by the injection of polyriboinosinic polyribocytidylic acid (data not shown). These data suggest that Hrs plays a crucial role in the degradation of ubiquitinated proteins in neural cells.

Expression Pattern of Glutamate Receptors, PSD-95, and p62

Because Hrs binds to ubiquitinated receptors and sorts them into lysosomes through multivesicular bodies, we performed immunohistochemical analyses in the hippocampus for NR1 and NR2B, the major subunits of NR, and for GluR1, the major subunit of AMPAR. In *hrs*$^{loxP/loxP}$*;Synl-cre* mice, NR1-, NR2B-, and GluR1-positive aggregates were observed in the perikarya of CA3 pyramidal cells (Figure 9, A–L). We suspected that the PSD-95 that is abundant in virtually all mature excitatory glutaminergic synapses might also be involved in the glutamate receptor accumulation. Previous studies indicate that Hrs binds to PSD-95β[32] and that PSD-95 controls glutaminergic synapse function.[33] Nevertheless, PSD-95-positive aggregates were not detected in the *hrs*$^{loxP/loxP}$*;Synl-cre* mice (Figure 9, M–P). These data suggest that Hrs affects the degradation of NR and AMPAR without affecting PSD-95.

Because Hrs is involved in the autophagic pathway,[34] it was possible that insufficient autophagy-dependent protein degradation was the reason for the aggregation of ubiquitinated protein in the CA3 region. We therefore examined the expression of two proteins: LC3, a specific marker of autophagosomes, and p62, which is regulated by autophagy and thus accumulates when autophagy is insufficient.[35] Although LC3-positive vesicles could not be detected in either the control or Hrs mutant mouse brain (data not shown), aggregated p62 was clearly observed in the pyramidal cell perikarya in the CA3 subfield of the Hrs mutant (Figure 10, A–D). Consistent with data in Figure 7, signals detected by FK2, including mono-and polyubiquitinated proteins, were also observed in *hrs*$^{loxP/loxP}$*;Synl-cre* mice. Notably, p62, GluR1, and NR2B were co-localized with each other, as well as with the ubiquitinated proteins (Figure 10, E–L).

Figure 7. Ubiquitin-positive inclusions in the *hrs*$^{loxP/loxP}$*;Synl-cre* brain. Immunohistochemistry of hippocampal CA3 sections from *hrs*$^{+/+}$*;Synl-cre* (**A**, **C**, **E**, **G**, **I**, **K**) and *hrs*$^{loxP/loxP}$*;Synl-cre* (**B**, **D**, **F**, **H**, **J**, **L**) mice at various weeks of age, stained with an anti-ubiquitin antibody (1B3). **A** and **B**: Five weeks old, low magnification. **C** and **D**: Two weeks old. **E** and **F**: Three weeks old. **G** and **H**: Five weeks old. **I** and **J**: Eight weeks old. **K** and **L**: Sixteen weeks old. **Arrow** indicates ubiquitin-positive cells. **M**: Nissl- or ubiquitin-positive cells in the hippocampal CA3 subfield were counted in comparable areas for *hrs*$^{+/+}$*;Synl-cre* and *hrs*$^{loxP/loxP}$*;Synl-cre* mice. Data represent the mean ± SE of three mice. Scale bars = 50 μm. Original magnifications: ×100 (**A**, **B**); ×400 (**C**–**L**).

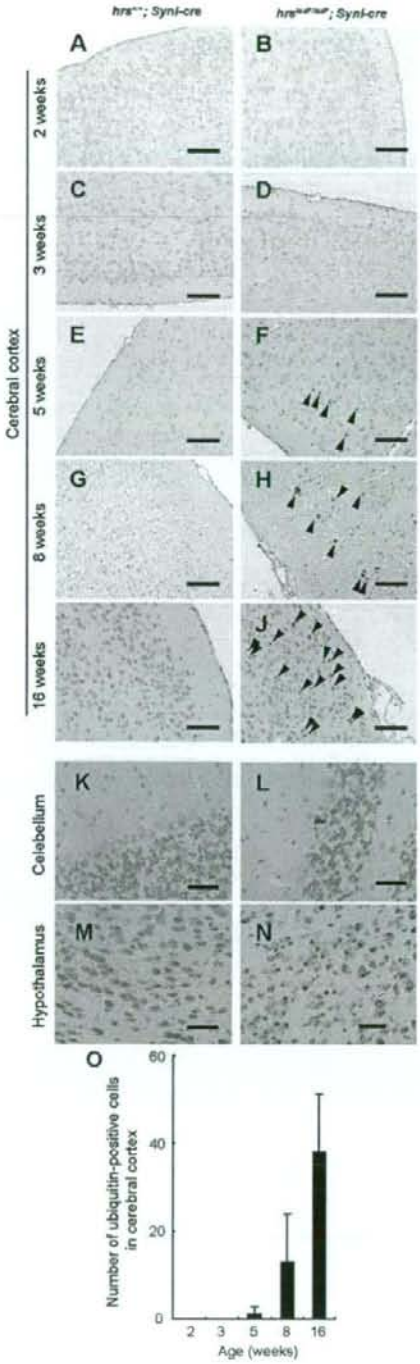

Learning Ability and Locomotor Activity Impairments in Hrs Mutant Mice

To investigate the effect of ubiquitinated protein accumulation in neural cells, behavioral analyses were performed with *hrs*$^{+/+}$;*Synl-cre* and *hrs*$^{loxP/loxP}$;*Synl-cre* mice. First, in an open field test, there were significant differences in the vertical (rearing) activity, but not in the horizontal activity, between the two groups (Figure 11, A and B). These results indicate that locomotor activity was impaired in the *hrs*$^{loxP/loxP}$;*Synl-cre* mice.

Next, because ubiquitinated proteins accumulated in the hypothalamus of the *hrs*$^{loxP/loxP}$;*Synl-cre* mice, we investigated the mental status of the two groups of mice by the forced swimming test, which is used to evaluate depression in rodents. In this test, a depressed state is induced in mice by forcing them to swim in an aquarium from which they cannot escape. The *Hrs*$^{loxP/loxP}$;*Synl-cre* mice showed a significantly longer duration of immobility (Figure 11C). To test whether *hrs*$^{loxP/loxP}$;*Synl-cre* mice had weaker muscles, we performed a wire-hanging test. No significant difference was observed between the two groups of mice in this test (Figure 11D). Footprint analysis also showed no difference between the two groups (Figure 11E). Collectively, these results indicate that the *hrs*$^{loxP/loxP}$;*Synl-cre* mice were in a depressive state.

Finally, we tested whether the loss of hippocampal CA3 neurons in the *hrs*$^{loxP/loxP}$;*Synl-cre* mice affected their learning ability. Mice were examined using a passive avoidance task. Twenty-four hours after training, the latency period for mice to enter the dark box was significantly shorter for the *hrs*$^{loxP/loxP}$;*Synl-cre* mice than for the *hrs*$^{+/+}$;*Synl-cre* mice (Figure 11F). This result is compatible with the observation of hippocampal neuron loss in the *hrs*$^{loxP/loxP}$;*Synl-cre* mice.

Discussion

In the present study, we detected the obvious accumulation of ubiquitinated proteins in 5-week-old *hrs*$^{loxP/loxP}$;*Synl-cre* brain, although neurodegeneration was not apparent in the hippocampus until after 8 weeks, suggesting that the aggregation of ubiquitinated proteins precedes neurodegeneration in these mice. We also found that ubiquitinated proteins in the cerebral cortex of *hrs*$^{loxP/loxP}$;*Synl-cre* mice increased with age, and that their learning ability was impaired, in accordance with the increase in ubiquitinated proteins. These findings reveal the importance of understanding Hrs' role in the mechanism of neurodegenerative diseases because some

Figure 8. Ubiquitin-positive inclusions in the *hrs*$^{loxP/loxP}$;*Synl-cre* brain. Immunohistochemistry of cerebral cortex (**A–J**), Purkinje cells (**K**, **L**), and hypothalamus (**M**, **N**) sections from *hrs*$^{+/+}$;*Synl-cre* (**A**, **C**, **E**, **G**, **I**, **K**, **M**) and *hrs*$^{loxP/loxP}$;*Synl-cre* (**B**, **D**, **F**, **H**, **J**, **L**, **N**) mice at various weeks of age, stained with an anti-ubiquitin antibody (1B3). **A** and **B**: Two weeks old. **C** and **D**: Three weeks old. **E**, **F**, **K**, and **L**: Five weeks old. **G** and **H**: Eight weeks old. **I**, **J**, **M**, and **N**: Sixteen weeks old. **Arrowheads** indicate ubiquitin-positive cells. **O**: Ubiquitin-positive cells in the cerebral cortex were counted in comparable areas for each *hrs*$^{loxP/loxP}$;*Synl-cre* mouse, and five fields were counted in each area for each mouse. Data represent the mean ± SE of three mice. Scale bars = 100 μm. Original magnifications, ×400.

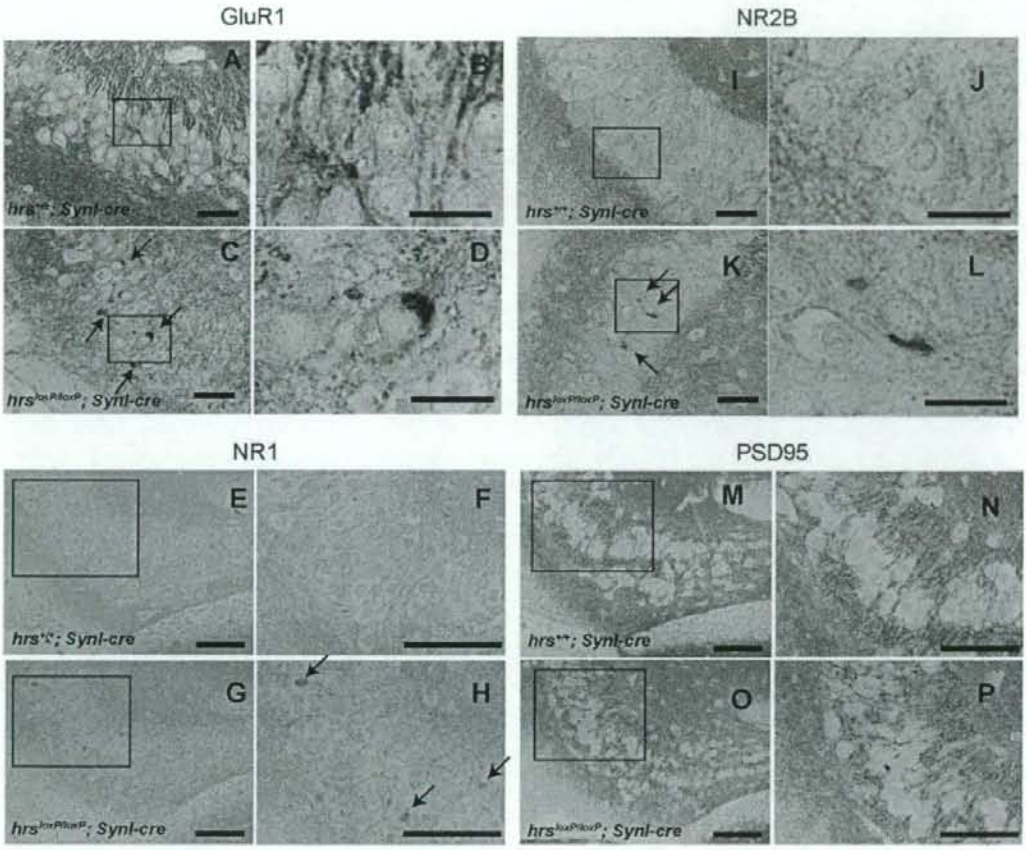

Figure 9. Immunohistochemistry of GluR1 (**A–D**), NR1 (**E–H**), NR2B (**I–L**), and PSD-95 (**M–P**) in the hippocampus CA3 subfield. Hippocampus sections from *hrs*$^{+/+}$*;Synl-cre* (**A**, **C**, **E**, **G**, **I**, **K**, **M**, **O**) and *hrs*$^{loxP/loxP}$*;Synl-cre* (**B**, **D**, **F**, **H**, **J**, **L**, **N**, **P**) 5-week-old mice were stained with GluR1-, NR1-, NR2B-, and PSD-95-specific antibodies. **Arrows** indicate protein aggregates. **Insets** show a higher magnification. Scale bars: 50 μm (**A**, **C**, **E–H**, **I**, **K**, **M–P**); 20 μm (**B**, **D**, **J**, **L**). Original magnifications, ×400.

ubiquitin-positive inclusions, such as phosphorylated tau and TDP-43, accumulate in the cerebral cortex, which results in the progressive loss of cognitive ability.[36] In this study, we could not detect the expression of phosphorylated tau in the cerebral cortex of *hrs*$^{loxP/loxP}$*;Synl-cre* mice using an anti-phosphorylated tau antibody (data not shown). Further study is required to reveal the relationship between the ESCRT proteins and neurodegenerative disease.

In neurons, NMDA receptor proteins usually concentrate at the postsynaptic density (PSD), a specialized apparatus beneath synapses that consists of receptors, scaffolding molecules, and signal-transduction enzymes. Synaptic transmission modulates the composition of the PSD, in part by the activity-dependent ubiquitination and degradation of PSD components.[37] The Mdm2-mediated ubiquitination of PSD-95 is critical for regulating the cell-surface expression of AMPA receptors in synaptic plasticity.[38] The overexpression of Hrs blocks the postsynaptic targeting of PSD-95β, which instead accumulates on large endosomal vesicles.[32] In this study, we found AMPAR- and NMDAR-positive aggregates in the hippocampus of *hrs*$^{loxP/loxP}$*;Synl-cre* mice, although their expression levels, except in the aggregates, were not significantly different between the *hrs*$^{loxP/loxP}$*;Synl-cre* and control mice. These observations suggest that the loss of hippocampal CA3 pyramidal neurons is not caused by excitotoxicity, but by protein aggregate-induced cellular toxicity. Generally, ESCRTs including Hrs were thought to regulate an endosomal pathway, not a proteasomal pathway.[11] Thus, we conclude that the loss of Hrs impairs the lysosome-dependent degradative pathway, thereby advancing the accumulation of ubiquitinated proteins, including glutamate receptors, resulting in neurodegeneration. However, we cannot exclude the possibility that we failed to detect altered CA3 pyramidal neurons in the *hrs*$^{loxP/loxP}$*;Synl-cre* mice.

Endosomes are major targets of genetic and epigenetic pathogenic factors in many neurodegenerative diseases.[39] In Huntington's disease, the expansion of a

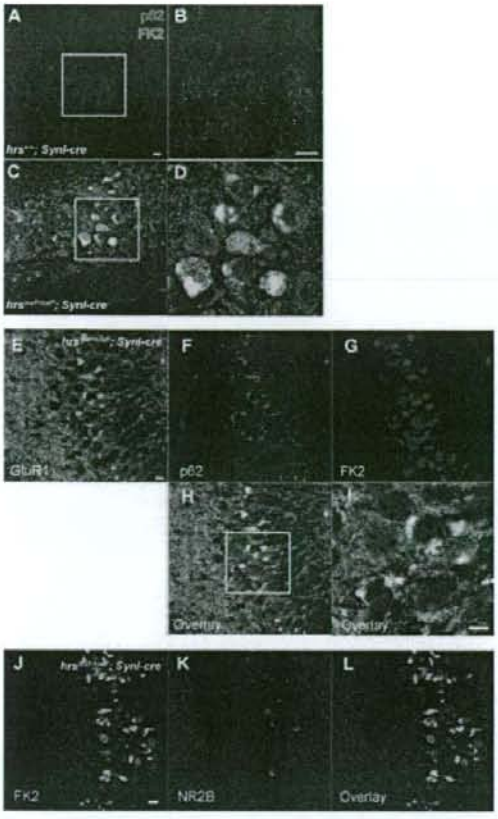

Figure 10. Immunohistochemistry of p62, FK2, GluR1, and NR2B in the hippocampus CA3 subfield. **A–D:** Aggregated p62 (red) and ubiquitinated proteins (green) were observed in the $hrs^{loxP/loxP}$;*Synl-cre* mice (**C**, **D**), but not in the $hrs^{+/+}$;*Synl-cre* mice (**A**, **B**). p62 was co-localized with ubiquitinated proteins (yellow). **E–L:** GluR1 and NR2B were also co-localized with p62 and FK2 in the $hrs^{loxP/loxP}$;*Synl-cre* mice. Scale bars = 10 μm. Original magnifications, ×400.

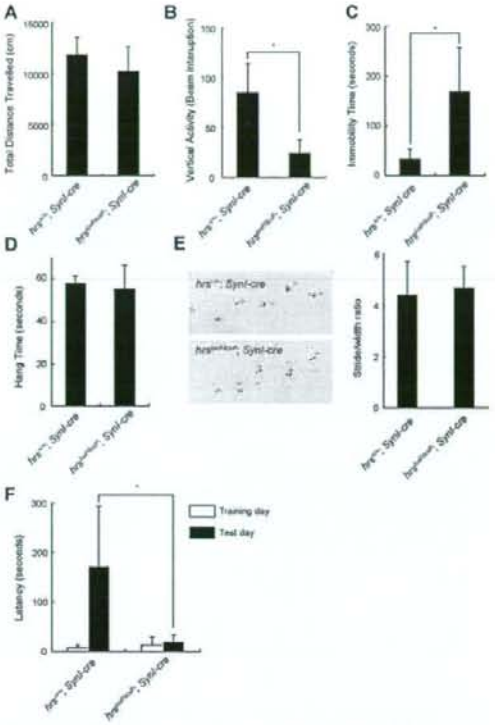

Figure 11. Behavioral examinations. **A** and **B:** The open-field activity test. Data are averages ± standard errors ($n = 10$) for the total distance (**A**) and vertical activity (**B**) of the $hrs^{+/+}$;*Synl-cre* and $hrs^{loxP/loxP}$;*Synl-cre* mice for 30 minutes. **C:** Increase of immobility time in the forced swimming test in the $hrs^{loxP/loxP}$;*Synl-cre* mice. Values are expressed as means ± standard errors ($n = 10$). **D:** Wire hanging test. $Hrs^{+/+}$;*Synl-cre* and $hrs^{loxP/loxP}$;*Synl-cre* mice were tested ($n = 10$). **E: Left**, paw placement records of 12-week-old mice; **right**, stride lengths corrected for paw base widths (stride/width ratio) of $hrs^{loxP/loxP}$;*Synl-cre* and $hrs^{+/+}$;*Synl-cre* littermate mice. Values are expressed as means ± standard errors of three mice. **F:** Loss of memory function of the $hrs^{loxP/loxP}$;*Synl-cre* mice in the step-through passive avoidance test. Data represent means ± standard errors of the step-through latency period ($n = 10$). Statistical differences between groups were determined by Student's *t*-test. $^*P < 0.05$.

polyglutamate tract in huntingtin (Htt) causes neuronal loss in the striatum and cortex.[40] Mutant Htt is believed to promote cell death in several ways that involve endosome dysfunction, and Htt normally associates with HIP1, a protein that co-localizes on early endosomes with its ligand Hrs.[41] Recent studies indicate that ESCRTs not only facilitate the trafficking of ubiquitylated proteins from endosomes to lysosomes, but play a critical role in autophagy; ESCRT III dysfunction causes autophagosome accumulation and neurodegeneration because of an abnormal fusion process between autophagosomes and endosomal compartments or lysosomes.[17,42] Moreover, autophagy is essential for the survival of neural cells, and its impairment is implicated in the pathogenesis of neurodegenerative disorders involving ubiquitin-containing inclusion bodies.[17,43,44] In $hrs^{loxP/loxP}$;*Synl-cre* mice, we found that ubiquitinated proteins accumulated in the hippocampus, which is similar to the finding for autophagy-deficient mice.[43,44] In this context, we previously demonstrated that Hrs plays a crucial role in autophagosome maturation.[34] Although we have not yet obtained direct evidence for it, it appears that the autophagic pathway is impaired in the hippocampal CA3 subfields of the $hrs^{loxP/loxP}$;*Synl-cre* mice, because p62, which is degraded by the autophagic pathway,[44] was among the accumulated proteins. Further study will be required to elucidate the function of Hrs in autophagy by using other organ-specific Cre transgenic mice.

It was striking that the loss of pyramidal neurons by Hrs depletion occurred only in the hippocampal CA3 subfield. It was also interesting that NR accumulated only in the CA3, and not in the CA1 subfield, even though NR1, a common subunit of NR,[45] is distributed in both CA1 and CA3. We expect that one of the following ideas will explain this selective phenotype: First, the expression of *hrs* is higher in the CA3 subfield than in CA1 (Figure 1, B and C). Second, certain cargos that are critical for neural

survival and sensitive to Hrs-dependent sorting and degradation may be restricted to CA3. Further study will be required to elucidate the reason for this specificity of Hrs-dependent neurodegeneration.

In severely depressed patients, emotional arousal, cognitive abnormality, and vulnerability to psychotic episodes are linked to hypothalamic-pituitary-adrenal axis activity.[46] Excessive stimulation of the axis is implicated in depression, and hyperactivity of the hypothalamic-pituitary-adrenal axis is observed in the majority of patients with depression.[47] We found that *hrs*$^{loxP/loxP}$*;Synl-cre* mice showed more immobility than controls in a forced swimming test, and that ubiquitinated proteins accumulated in the hypothalamus of these mice, although hypothalamic neurons were not lost. These observations suggest that ubiquitinated proteins in the neural cells of *hrs*$^{loxP/loxP}$*;Synl-cre* mice might impair hypothalamic function and the hypothalamic-pituitary-adrenal axis. We also found that the loss of Hrs markedly impaired the retention of passive avoidance behavior 24 hours after the training trial. A previous study showed that CA3 NMDAR function is absent during memory formation in CA3-NR1 KO mice,[48] which is similar to the phenotype of Hrs mutant mice. Our data are compatible with this study.

The present study indicates that Hrs plays a pivotal role in the survival of neural cells through its involvement in the degradation pathway for ubiquitinated proteins. Although it is still unknown whether Hrs selectively recognizes harmful gene products associated with neurodegenerative disorders such as Huntington's, Parkinson's, and Alzheimer's disease, our Hrs mutant mice provide an excellent animal model system for studying the molecular mechanisms of neurodegenerative diseases.

Acknowledgments

We thank Dr. Jamey D. Marth for the Synapsin-I Cre transgenic mice; Kazuhiko Yanai and Eiko Sakurai for their help with the behavioral examinations; Drs. Hiromu Yawo, Yasuto Itoyama, Ichiro Sora, and Toshio Watanabe for discussion; and Ms. Rie Ito for technical assistance.

References

1. Ballatore C, Lee VM, Trojanowski JQ: Tau-mediated neurodegeneration in Alzheimer's disease and related disorders. Nat Rev Neurosci 2007, 8:663–672
2. Trojanowski JQ, Lee VM: "Fatal attractions" of proteins: a comprehensive hypothetical mechanism underlying Alzheimer's disease and other neurodegenerative disorders. Ann N Y Acad Sci 2000, 924:62–67
3. Rubinsztein DC: The roles of intracellular protein-degradation pathways in neurodegeneration. Nature 2006, 443:780–786
4. Aarts MM, Tymianski M: Molecular mechanisms underlying specificity of excitotoxic signaling in neurons. Curr Mol Med 2004, 4:137–147
5. Mattson MP: Excitotoxic and excitoprotective mechanisms: abundant targets for the prevention and treatment of neurodegenerative disorders. Neuromolecular Med 2003, 3:65–94
6. Moghaddam B: Bringing order to the glutamate chaos in schizophrenia. Neuron 2003, 40:881–884
7. Tzschentke TM: Glutamatergic mechanisms in different disease states: overview and therapeutical implications—an introduction. Amino Acids 2002, 23:147–152
8. Mori H, Mishina M: Structure and function of the NMDA receptor channel. Neuropharmacology 1995, 34:1219–1237
9. Kato A, Rouach N, Nicoll RA, Bredt DS: Activity-dependent NMDA receptor degradation mediated by retrotranslocation and ubiquitination. Proc Natl Acad Sci USA 2005, 102:5600–5605
10. Schaefer H, Rongo C: KEL-8 is a substrate receptor for CUL3-dependent ubiquitin ligase that regulates synaptic glutamate receptor turnover. Mol Biol Cell 2006, 17:1250–1260
11. Babst M: A protein's final ESCRT. Traffic 2005, 6:2–9
12. Raiborg C, Rusten TE, Stenmark H: Protein sorting into multivesicular endosomes. Curr Opin Cell Biol 2003, 15:446–455
13. Komada M, Soriano P: Hrs, a FYVE finger protein localized to early endosomes, is implicated in vesicular traffic and required for ventral folding morphogenesis. Genes Dev 1999, 13:1475–1485
14. Miura S, Takeshita T, Asao H, Kimura Y, Murata K, Sasaki Y, Hanai JI, Beppu H, Tsukazaki T, Wrana JL, Miyazono K, Sugamura K: Hgs (Hrs), a FYVE domain protein, is involved in Smad signaling through cooperation with SARA. Mol Cell Biol 2000, 20:9346–9355
15. Ehlers MD: Deconstructing the axon: Wallerian degeneration and the ubiquitin-proteasome system. Trends Neurosci 2004, 27:3–6
16. Filimonenko M, Stuffers S, Raiborg C, Yamamoto A, Malerod L, Fisher EM, Isaacs A, Brech A, Stenmark H, Simonsen A: Functional multivesicular bodies are required for autophagic clearance of protein aggregates associated with neurodegenerative disease. J Cell Biol 2007, 179:485–500
17. Lee JA, Beigneux A, Ahmad ST, Young SG, Gao FB: ESCRT-III dysfunction causes autophagosome accumulation and neurodegeneration. Curr Biol 2007, 17:1561–1567
18. Yagi T, Tokunaga T, Furuta Y, Nada S, Yoshida M, Tsukada T, Saga Y, Takeda N, Ikawa Y, Aizawa S: A novel ES cell line, TT2, with high germline-differentiating potency. Anal Biochem 1993, 214:70–76
19. Dymecki SM: Flp recombinase promotes site-specific DNA recombination in embryonic stem cells and transgenic mice. Proc Natl Acad Sci USA 1996, 93:6191–6196
20. Zhu Y, Romero MI, Ghosh P, Ye Z, Charnay P, Rushing EJ, Marth JD, Parada LF: Ablation of NF1 function in neurons induces abnormal development of cerebral cortex and reactive gliosis in the brain. Genes Dev 2001, 15:859–876
21. Tanaka N, Kaneko K, Asao H, Kasai H, Endo Y, Fujita T, Takeshita T, Sugamura K: Possible involvement of a novel STAM-associated molecule "AMSH" in intracellular signal transduction mediated by cytokines. J Biol Chem 1999, 274:19129–19135
22. Asao H, Sasaki Y, Arita T, Tanaka N, Endo K, Kasai H, Takeshita T, Endo Y, Fujita T, Sugamura K: Hrs is associated with STAM, a signal-transducing adaptor molecule. Its suppressive effect on cytokine-induced cell growth. J Biol Chem 1997, 272:32785–32791
23. Abe M, Fukaya M, Yagi T, Mishina M, Watanabe M, Sakimura K: NMDA receptor GluRepsilon/NR2 subunits are essential for postsynaptic localization and protein stability of GluRzeta1/NR1 subunit. J Neurosci 2004, 24:7292–7304
24. Fukaya M, Kato A, Lovett C, Tonegawa S, Watanabe M: Retention of NMDA receptor NR2 subunits in the lumen of endoplasmic reticulum in targeted NR1 knockout mice. Proc Natl Acad Sci USA 2003, 100:4855–4860
25. Nagy GG, Al-Ayyan M, Andrew D, Fukaya M, Watanabe M, Todd AJ: Widespread expression of the AMPA receptor GluR2 subunit at glutamatergic synapses in the rat spinal cord and phosphorylation of GluR1 in response to noxious stimulation revealed with an antigen-unmasking method. J Neurosci 2004, 24:5766–5777
26. Yamada M, Takeshita T, Miura S, Murata K, Kimura Y, Ishii N, Nose M, Sakagami H, Kondo H, Tashiro F, Miyazaki JI, Sasaki H, Sugamura K: Loss of hippocampal CA3 pyramidal neurons in mice lacking STAM1. Mol Cell Biol 2001, 21:3807–3819
27. Schaeren-Wiemers N, Gerfin-Moser A: A single protocol to detect transcripts of various types and expression levels in neural tissue and cultured cells: in situ hybridization using digoxigenin-labelled cRNA probes. Histochemistry 1993, 100:431–440
28. Chen Z, Sakurai E, Hu W, Jin C, Kiso Y, Kato M, Watanabe T, Wei E, Yanai K: Pharmacological effects of carcinine on histaminergic neurons in the brain. Br J Pharmacol 2004, 143:573–580
29. Sango K, McDonald MP, Crawley JN, Mack ML, Tifft CJ, Skop E, Starr CM, Hoffmann A, Sandhoff K, Suzuki K, Proia RL: Mice lacking both

subunits of lysosomal beta-hexosaminidase display gangliosidosis and mucopolysaccharidosis. Nat Genet 1996, 14:348–352
30. Zomkowski AD, Santos AR, Rodrigues AL: Putrescine produces antidepressant-like effects in the forced swimming test and in the tail suspension test in mice. Prog Neuropsychopharmacol Biol Psychiatry 2006, 30:1419–1425
31. Klapdor K, Dulfer BG, Hammann A, Van der Staay FJ: A low-cost method to analyse footprint patterns. J Neurosci Methods 1997, 75:49–54
32. Chetkovich DM, Bunn RC, Kuo SH, Kawasaki Y, Kohwi M, Bredt DS: Postsynaptic targeting of alternative postsynaptic density-95 isoforms by distinct mechanisms. J Neurosci 2002, 22:6415–6425
33. Béique JC, Lin DT, Kang MG, Aizawa H, Takamiya K, Huganir RL: Synapse-specific regulation of AMPA receptor function by PSD-95. Proc Natl Acad Sci USA 2006, 103:19535–19540
34. Tamai K, Tanaka N, Nara A, Yamamoto A, Nakagawa I, Yoshimori T, Ueno Y, Shimosegawa T, Sugamura K: Role of Hrs in maturation of autophagosomes in mammalian cells. Biochem Biophys Res Commun 2007, 360:721–727
35. Komatsu M, Waguri S, Koike M, Sou YS, Ueno T, Hara T, Mizushima N, Iwata J, Ezaki J, Murata S, Hamazaki J, Nishito Y, Iemura S, Natsume T, Yanagawa T, Uwayama J, Warabi E, Yoshida H, Ishii T, Kobayashi A, Yamamoto M, Yue Z, Uchiyama Y, Kominami E, Tanaka K: Homeostatic levels of p62 control cytoplasmic inclusion body formation in autophagy-deficient mice. Cell 2007, 131:1149–1163
36. Forman MS, Trojanowski JQ, Lee VM: Neurodegenerative diseases: a decade of discoveries paves the way for therapeutic breakthroughs. Nat Med 2004, 10:1055–1063
37. Ehlers MD: Activity level controls postsynaptic composition and signaling via the ubiquitin-proteasome system. Nat Neurosci 2003, 6:231–242
38. Colledge M, Snyder EM, Crozier RA, Soderling JA, Jin Y, Langeberg LK, Lu H, Bear MF, Scott JD: Ubiquitination regulates PSD-95 degradation and AMPA receptor surface expression. Neuron 2003, 40:595–607
39. Nixon RA: Endosome function and dysfunction in Alzheimer's disease and other neurodegenerative diseases. Neurobiol Aging 2005, 26:373–382
40. Vonsattel JP, DiFiglia M: Huntington disease. J Neuropathol Exp Neurol 1998, 57:369–384
41. Metzler M, Li B, Gan L, Georgiou J, Gutekunst CA, Wang Y, Torre E, Devon RS, Oh R, Legendre-Guillemin V, Rich M, Alvarez C, Gertsenstein M, McPherson PS, Nagy A, Wang YT, Roder JC, Raymond LA, Hayden MR: Disruption of the endocytic protein HIP1 results in neurological deficits and decreased AMPA receptor trafficking. EMBO J 2003, 22:3254–3266
42. Rusten TE, Vaccari T, Lindmo K, Rodahl LM, Nezis IP, Sem-Jacobsen C, Wendler F, Vincent JP, Brech A, Bilder D, Stenmark H: ESCRTs and Fab1 regulate distinct steps of autophagy. Curr Biol 2007, 17:1817–1825
43. Hara T, Nakamura K, Matsui M, Yamamoto A, Nakahara Y, Suzuki-Migishima R, Yokoyama M, Mishima K, Saito I, Okano H, Mizushima N: Suppression of basal autophagy in neural cells causes neurodegenerative disease in mice. Nature 2006, 441:885–889
44. Komatsu M, Waguri S, Chiba T, Murata S, Iwata J, Tanida I, Ueno T, Koike M, Uchiyama Y, Kominami E, Tanaka K: Loss of autophagy in the central nervous system causes neurodegeneration in mice. Nature 2006, 441:880–884
45. Köhr G: NMDA receptor function: subunit composition versus spatial distribution. Cell Tissue Res 2006, 326:439–446
46. de Kloet ER, Derijk RH, Meijer OC: Therapy insight: is there an imbalanced response of mineralocorticoid and glucocorticoid receptors in depression? Nat Clin Pract Endocrinol Metab 2007, 3:168–179
47. Berton O, Nestler EJ: New approaches to antidepressant drug discovery: beyond monoamines. Nat Rev Neurosci 2006, 7:137–151
48. Nakazawa K, Quirk MC, Chitwood RA, Watanabe M, Yeckel MF, Sun LD, Kato A, Carr CA, Johnston D, Wilson MA, Tonegawa S: Requirement for hippocampal CA3 NMDA receptors in associative memory recall. Science 2002, 297:211–218

Low-intensity ultrasound and microbubbles enhance the antitumor effect of cisplatin

Yukiko Watanabe,[1] Atsuko Aoi,[2] Sachiko Horie,[1] Noriko Tomita,[1] Shiro Mori,[3] Hidehiro Morikawa,[3] Yasuhiro Matsumura,[4] Georges Vassaux[5,6] and Tetsuya Kodama[1,7]

[1]Graduate School of Biomedical Engineering, [2]Graduate School of Dentistry, Tohoku University, [3]Tohoku University Hospital, Sendai, Miyagi 980-8575; [4]Investigative Treatment Division, Research Center for Innovative Oncology, National Cancer Center Hospital East, Kashiwa, Chiba 277-8577, Japan; [5]CIC-INSERM 00-04, EA 4274, CHU Hôtel Dieu, Nantes, cedex 1; [6]Institut des Maladies de l'Appareil Digestif, CHU Hotel Dieu, Nantes, cedex 1, France

(Received July 18, 2008/Revised August 21, 2008/Accepted August 24, 2008/Online publication November 19, 2008)

Cell permeabilization using microbubbles (MB) and low-intensity ultrasound (US) have the potential for delivering molecules into the cytoplasm. The collapsing MB and cavitation bubbles created by this collapse generate impulsive pressures that cause transient membrane permeability, allowing exogenous molecules to enter the cells. To evaluate this methodology *in vitro* and *in vivo*, we investigated the effects of low-intensity 1-MHz pulsed US and MB combined with *cis*-diamminedichloroplatinum (II) (CDDP) on two cell lines (Colon 26 murine colon carcinoma and EMT6 murine mammary carcinoma) *in vitro* and *in vivo* on severe combined immunodeficient mice inoculated with HT29-luc human colon carcinoma. To investigate *in vitro* the efficiency of molecular delivery by the US and MB method, calcein molecules with a molecular weight in the same range as that of CDDP were used as fluorescent markers. Fluorescence measurement revealed that approximately 10^6–10^7 calcein molecules per cell were internalized. US–MB-mediated delivery of CDDP in Colon 26 and EMT6 cells increased cytotoxicity in a dose-dependent manner and induced apoptosis (nuclear condensation and fragmentation, and increase in caspase-3 activity). *In vivo* experiments with xenografts (HT29-luc) revealed a very significant reduction in tumor volume in mice treated with CDDP + US + MB compared with those in the US + CDDP groups for two different concentrations of CDDP. This finding suggests that the US–MB method combined with chemotherapy has clinical potential in cancer therapy. (*Cancer Sci* 2008; 99: 2525–2531)

Microbubbles (MB) have been developed as ultrasound (US) contrast agents with a diameter of less than 10 μm. The components of their shell membrane vary (albumin, lipid, or polymer), and gases such as air or perfluorocarbons are internalized in them.[1–3] These bubbles oscillate non-linearly in an US field and emit harmonic and subharmonic acoustic signals, thereby enabling differentiation between acoustic scattering and vascular signatures. In addition, because these bubbles behave similar to red blood cells, they have been used to evaluate the blood pool and blood flow at the microvascular level.[4]

Microbubbles collapse in the presence of low-intensity US. There is evidence that impulsive pressures generated by either collapsing MB[5,6] or the cavitation bubbles created by this collapse may permeabilize the plasma membrane of neighboring cells.[7,8] This process results in the diffusion of nearby exogenous molecules into the cytoplasm and a subsequent biological response.[8–11] Because these impulsive pressures can be induced by high-intensity US,[12,13] substantial thermal and mechanical side effects can be reduced using the US–MB method.

The US–MB method is non-toxic and non-immunogenic, and allows local or systemic administration. This method can be used to deliver exogenous molecules into dividing and non-dividing cells and has been investigated as an approach for *in vivo* gene transfer and molecular delivery.[14–16] In any case, the efficiency of molecular delivery depends on the size of the molecules to be delivered.[17,18] The amount of molecules increases with decreasing molecular weight. Thus, it is expected that this methodology will be useful for therapeutic strategies involving drugs with small molecular sizes. Cis-diamminedichloroplatinum (II) (cisplatin; CDDP) is one of the most effective and commonly used chemotherapeutics, possessing a molecular weight of 300. CDDP has been used for the treatment of many solid tumors, including those of the ovaries, testicles, bladder, lung, and head and neck.[19] Increasing CDDP penetration into the tumor cells could further improve its therapeutic efficacy. In the present study, we estimated the number of CDDP molecules internalized by the US–MB method using calcein molecules with molecular weights in the same range as that of CDDP as fluorescent markers. Subsequently, we assessed the therapeutic potential of the combination of CDDP and US with MB *in vitro* and *in vivo* and demonstrated that this combination induces apoptotic effects, and increases the therapeutic efficacy.

Materials and Methods

In vitro and *in vivo* studies were carried out in accordance with the ethical guidelines approved by Tohoku University.

Cell preparation. Human embryonic kidney (293T) cells were a generous gift from Dr Ono of Tohoku University. Murine mammary carcinoma (EMT6) cells were obtained from the American Type Culture Collection (Rockville, MD, USA). Murine colon carcinoma (Colon 26) cells were obtained from the Cell Resource Center for Biomedical Research of the Institute of Development, Aging and Cancer, Tohoku University (Sendai, Japan). Human colon carcinoma (HT-29-luc) cells stably transfected with a plasmid carrying the firefly luciferase gene driven by a cytomegalovirus promoter were obtained from Xenogen (Alameda, CA, USA). Colon 26 and HT-29-luc cells were cultured under standard conditions in RPMI-1640 medium supplemented with 10% heat-inactivated fetal bovine serum (Invitrogen, Carlsbad, CA, USA) and 1% L-glutamine–penicillin–streptomycin (Sigma-Aldrich, St Louis, MO, USA), whereas 293T and EMT6 cells were cultured in Dulbecco's modified Eagle's medium (Sigma-Aldrich) containing the same supplements as those added to the RPMI-1640 medium. HT29-luc cells were selected in 1 mg/mL geneticin (G418) (Sigma-Aldrich). Cells cultured in a 10-cm culture dish were maintained in a humidified incubator at 37°C under an atmosphere containing 5% CO_2 and

[7]To whom correspondence should be addressed.
E-mail: kodama@bme.tohoku.ac.jp

doi: 10.1111/j.1349-7006.2008.00989.x

95% air. The total cell counts and viability were counted in a hemocytometer by the trypan blue dye exclusion method[20] prior to US exposure. Only cells in their exponential growth phase with a viability ≥99% were used for the study.

Microbubbles. MB were created in an aqueous dispersion of 2 mg/mL 1,2-distearoyl-sn-glycero-3-phosphocholine (Avanti Polar Lipids, Alabaster, AL, USA) and 1 mg/mL polyethylene glycol 40 stearate (Sigma-Aldrich) using a 20-kHz sonicator (Vibra Cell; Sonics and Materials, Danbury, CT, USA) in the presence of C_3F_8 gas.[21] The lipid molecules that formed components of the MB surface were confirmed by staining the molecules with 3 μmol/L FM1-43 (excitation 479 nm, emission 598 nm; Molecular Probes, Eugene, OR, USA) and observing them under an inverted microscope (IX81; Olympus, Tokyo, Japan). The peak diameter and the zeta potential of the MB were determined to be 1272 ± 163 nm ($n = 7$) and −4.1 ± 0.85 mV ($n = 3$), respectively, by using a laser diffraction particle size analyzer (particle range 0.6 nm–7 μm; ELSZ-2; Otsuka Electronics, Osaka, Japan).

Ultrasound exposure. Three 1-MHz submersible US probes were used. A 12-mm (Fuji Ceramics, Fujinomiya, Japan) and a 30-mm diameter probe (BFC Applications, Fujisawa, Japan) were used for the *in vitro* experiments, whereas 38-mm diameter probes (Fuji Ceramics) were used for the *in vivo* experiments. Each probe was placed in the test chamber (380 mm × 250 mm × 130 mm) that was previously filled with tap water. Signals of 1 MHz were generated by a multifunction synthesizer (WF1946A; NF Co., Yokohama, Japan) and amplified with a high-speed bipolar amplifier (HSA4101; NF Co.). The pressure values were measured using a polyvinylidene fluoride (PVDF) needle hydrophone (PVDF-Z44-1000; Specialty Engineering Associates, Soquel, CA, USA) at a stand-off distance of 1 mm from the transducer surface by using a stage control system (Mark-204-MS; Sigma Koki, Tokyo, Japan). The signals from both the amplifier and the hydrophone were recorded onto a digital phosphor oscilloscope (Wave Surfer 454, 500 MHz, 1 MΩ [16 pF]; LeCroy Co., Chestnut, NY, USA) in top water degassed with transducer (SPN-620) generated by ultrasonic generator α2 (GP-622D) (Tiyoda Electric Co., Chikuma, Japan). The positive and negative peak values of the pressures were the same. Two intensities, 0.5 and 1.0 W/cm^2, were used in the *in vitro* experiments. The duty cycle was 50%, the number of pulses was 2000, the pulse repletion frequency was 250 Hz, and the exposure time was 10 s. For the *in vivo* experiments, the intensity was 3.0 W/cm^2, the duty cycle was 20%, the number of pulses was 200; the pulse repletion frequency was 1000 Hz, and the exposure time was 60 s. The intensity was defined as the average rate of flow of energy through a unit area placed normal to the direction of propagation.

***In vitro* quantization of calcein uptake.** The 293T cells (5×10^4 cells/well) were seeded in complete medium onto 48-well plates and incubated at 37°C in a 5% CO_2 incubator. On the next day, the medium was replaced with fresh medium containing 200 μmol/L calcein (molecular weight 622) (excitation 494 nm, emission 517 nm; Sigma-Aldrich) with and without MB (10% v/v). After US exposure for 10 s, the cells were washed with phosphate-buffered saline (PBS), trypsinized, and collected in a 15-mL conical tube. Thereafter, the cells were washed three times and transferred to a 1.5-mL conical tube in which they were pelleted. The pellets were lysed in 200 μL reporter lysis buffer (Promega, Madison, WI, USA) and subsequently frozen at −80°C for 15 min. The cells were thawed on ice. Each cell lysate was centrifuged at 12 000*g* for 2 min to pellet the cell debris. Twenty microliters of the supernatant was examined for the uptake of fluorescent molecules using Mx3000P software (Stratagene, La Jolla, CA, USA). The fluorescence of these molecules was excited using a quartz tungsten halogen lamp (350–750 nm), and the emission was collected with a 492–516-nm bandpass filter. The fluorescence data were analyzed with MxPro QPCR Software (Stratagene). The total protein content from an aliquot of each sample of supernatant was calculated by establishing albumin standard curves (BCA protein assay kit; Pierce, Rockford, IL, USA). In addition, two other standard curves were utilized: one to determine the total protein content of the cells, and the other to determine the concentration and intensity of the fluorescence. The experiment was carried out with samples and standards in duplicate, and the absorption of the protein was measured at 562 nm using a plate reader (Sunrise; Tecan Austria, Salzburg, Austria) with the data analysis software LS-Plate manager RD 2001 (Win) (Sunrise). The number of equivalent fluorescent molecules per cell was determined from the calibration curves.

Imaging of confocal fluorescence microscopy. The 293T cells (5×10^4 cells/well) were seeded in complete medium onto alternate 48-well plates to prevent US exposure of neighboring cells.[8] On the next day, the medium was replaced with fresh medium (110 μL) containing calcein (200 μmol/L) with and without MB (10% v/v). After US exposure of 10 s, the plates were incubated for 24 h. Thereafter, the cells were washed three times with PBS and trypsinized. Finally, the cell pellet was resuspended in 60 μL propidium iodide (PI) (excitation 536 nm, emission 617 nm; Molecular Probes) (0.7 μg/mL) and incubated at room temperature for 10–15 min. The calcein and PI fluorescence intensities were determined with a confocal microscope (FV1000; Olympus). A ×60 oil-immersion objective lens with a numerical aperture of 1.25 was used. Calcein and PI fluorescence were excited with the 488-nm line of an argon laser. The laser excitation beam was directed to the specimen through a 488-nm dichroic beam splitter. The emitted fluorescence was collected through a 510–550-nm bandpass emission filter in the green channel and a 580-nm longpass filter in the red channel. Computer-generated images of 1-μm optical sections were obtained at the approximate geometric center of the cell as determined by repeated optical sectioning.

***In vitro* delivery of CDDP.** CDDP (molecular weight 300) was donated by Nihon Kayaku (Tokyo, Japan). Colon 26 and EMT6 cells were seeded in complete medium onto 10-cm culture dishes. Both cells were trypsinized, counted, and transferred into 15-mL round tubes at concentrations of 5×10^5 and 3×10^5 cells/mL, respectively. For control samples, 1 mL complete medium was used as the sample solution; for treated samples, the sample solution was mixed with 800 μL complete medium, 100 μL CDDP solution (0.5–1.0 mmol/L), and 100 μL MB solution (7% v/v). Each tube was positioned above a 30-mm diameter US probe that was immersed in tap water and exposed to US (10 s; 0.5 W/cm^2). After exposure, 4 mL PBS was added to each tube and centrifuged for 5 min at 4°C (350*g*). The cells were washed twice with PBS and subsequently seeded in 1 mL complete medium onto 24-well plates. The plates were incubated for 24 h at 37°C in a 5% CO_2 incubator. The cell viability was determined by a 3-(4,5-dimethylthiazol-2-yl)-2, 5-diphenyltetrazolium bromide (MTT) assay as described previously.[22] Each experiment was carried out with five samples. For each experiment, the mean percentage of treated samples was divided by the mean percentage of control samples to obtain the survival fraction. The mean of five survival fractions was calculated for each condition. The survival fraction of each cell line was measured at the CDDP concentration at which the highest statistical significance was obtained.

***In vitro* analysis of apoptosis.** Colon 26 (5×10^4 cells/well) cells were seeded onto alternate 48 wells to prevent the US exposure of neighboring cells.[8] The medium was replaced with fresh medium (110 μL) containing CDDP (1.5 mg) with and without MB (7% v/v). After US exposure, the plates were incubated for 1 h in a 5% CO_2 incubator, supplemented with 390 μL complete medium; subsequently, the plates were incubated for an additional 24 h at 37°C in the same incubator. The final

doi: 10.1111/j.1349-7006.2008.00989.x

concentration of CDDP was 10 μmol/L. The cell viability was determined by an MTT assay as described previously.[22] Staining with 4′,6-diamidino-2-phenylindole (DAPI; Sigma-Aldrich) was carried out for observing nuclear condensation and fragmentation. Twenty-four hours after the addition of CDDP, the cells were washed with PBS, stained with 100 μL DAPI (100 ng/mL) solution, and observed under an inverted microscope (IX 81). DAPI fluorescence of the cell nuclei was visualized by excitation at 330–385 nm with a 420-nm barrier filter. For determining the induction of apoptotic mediator proteins, caspase-3 activity was measured using a colorimetric assay kit (Medical and Biological Laboratories, Woburn, MA, USA) 24 h after the treatment. In brief, the treated cells were collected from 12 wells of the 48-well plates and suspended in cell lysis buffer. Aliquots of protein were incubated in a reaction buffer containing 10 mmol/L dithiothreitol (DTT) at 37°C for 1 h. A p-nitroaniline-conjugated synthetic peptide was used as the substrate. The caspase activity was calculated by measuring the optic absorbance at 400 nm using a plate reader with the data analysis software LS-Plate manager RD 2001 (Win).

***In vivo* therapeutic effects.** To evaluate the antitumor effects of MB, the antitumor effects of CDDP + US and CDDP + US + MB were compared using xenografts of HT29-luc cells. Two CDDP concentrations (0.5 and 1.25 μg/g bodyweight) were used. HT29-luc cells (1×10^6 cells) in 100 μL saline were injected subcutaneously into the right and left flanks of 16 male severe combined immunodeficient mice aged 6–9 weeks (mouse bodyweight was set to 20 g). The mice were assigned randomly into two groups. On days 3, 7, and 10, all mice were injected intratumorally with the following assigned treatments. (i) Four mice received 20 μL CDDP (0.5 μg/μL bodyweight) with 80 μL saline per site following US exposure (CDDP + US), and four others received 20 μL CDDP (0.5 μg/μL bodyweight) with 30 μL saline and 50 μL MB per site following US exposure (CDDP + US + MB). (ii) Four mice received 50 μL CDDP (1.25 μg/μL bodyweight) with 50 μL saline per site following US exposure (CDDP + US), and four others received 50 μL CDDP (1.25 μg/μL bodyweight) with 50 μL MB per site following US exposure (CDDP + US + MB). The tumors were immersed in tap water with a temperature of 37°C, positioned just above the 38-mm diameter US probe, and exposed to US (3.0 W/cm^2, 60 s). Bioluminescence induced by CDDP + US + MB was normalized with that of CDDP + US at each concentration (0.5 and 1.25 μg/g bodyweight) on days 4, 7, 9, and 11 to provide the antitumor effects of MB.

Bioluminescence imaging. On days 4, 7, 9, and 11, the mice were anesthetized with isoflurane. Subsequently, they were injected intraperitoneally with luciferin (150 μg/g bodyweight) and placed on the *in vivo* imaging system (IVIS100; Xenogen). The bioluminescence signals were monitored at 10-s time intervals after 10 min luciferin administration. The signal intensity was quantified as the sum of all detected photon counts within the region of interest after subtraction of the measured background luminescence. The light intensity closely correlated with the tumor volume (EMT6-luc) up to 100 mm^3, at which point the tumor volume was calculated according to the formula $(\pi/6) \times (\text{width})^2 \times (\text{length})$.[21] In the present experiment, all tumors (HT29-luc) with a volume less than 100 mm^3 were subjected to treatment.

Statistical analysis. All measurements are expressed as mean ± SEM. An overall difference between the groups was determined by one-way analysis of variance (one-way ANOVA). When the one-way ANOVA results were significant for three samples, the differences between each group were estimated using the Tukey–Kramer test. Simple comparisons of the mean and SEM of the data were carried out using Student's *t*-test. The differences were considered to be significant at $P < 0.05$.

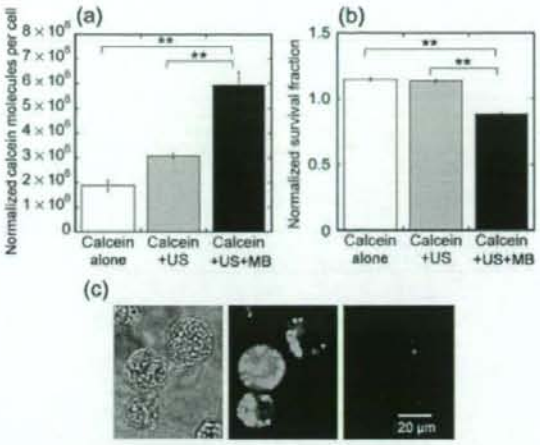

Fig. 1. Uptake of fluorescent molecules by 293T cells. (a) Mean fluorescence uptake under various conditions (calcein alone, calcein + ultrasound [US], and calcein + US + microbubbles [MB]). The calcein + US + MB condition results in a significant increase in the uptake of fluorescent molecules (6.0 ± 0.5 ¥ 106 molecules per cell) compared to calcein alone and calcein + US. Calcein alone (n = 4), calcein + US (n = 4), calcein + US + MB (n = 4). (b) Cell viability measured by the a 3-(4,5-dimethylthiazol-2-yl)-2, 5-diphenyltetrazolium bromide (MTT) assay. The survival fraction is decreased slightly by the effect of US + MB. Calcein alone (n = 4), calcein + US (n = 4), calcein + US + MB (n = 4). (c) Confocal microscopy showing differential interference contrast (left) and fluorescence images (middle) or representative viable 293T cells (right) exposed to US in the presence of MB. Propidium iodide (PI) staining was carried out with fluorescence staining in some cases to confirm that the cells that acquired calcein were viable and excluded PI. Scale bars = 20 mm. Ultrasound intensity 1.0 W/cm2; duty cycle 50%; number of pulses 2000; pulse repletion frequency 250 Hz; and exposure time 10 s. **P < 0.01.

Results

Uptake of fluorescent molecules. Calcein, which has a molecular weight of 622 (calculated stokes radius of 0.68),[23] was used as a fluorescent marker to evaluate small-molecule entry in cancer cells upon US–MB stimulation. As the molecular weight of CDDP is 300 (calculated stokes radius is 0.48 nm), calcein can be considered to represent a realistic marker of CDDP entry into tumor cells.

The exposure of cells to US in the presence of MB resulted in the delivery of 10^6–10^7 calcein molecules per cell (Fig. 1a). This represents a significant increase in the uptake of fluorescent molecules compared to calcein alone and calcein + US. Figure 1b shows that this effect was achieved with a very limited loss of cell viability that was measured by MTT assay, where the survival fraction rate due to MB alone was not investigated as it was found that MB alone did not contribute to cell viability.[24] To confirm that the calcein molecules actually entered the cytoplasm, confocal fluorescence microscopic analysis was carried out. Figure 1c shows the differential interference contrast and fluorescence images or the representative viable 293T cells exposed to US in the presence of MB. PI staining was also carried out with some instances of fluorescence staining to confirm that the cells that acquired calcein were viable and excluded PI. Some cells treated with US in the presence of MB demonstrated intense fluorescence distributed uniformly throughout the entire cell, whereas other cells demonstrated localized intense fluorescence (Fig. 1c).

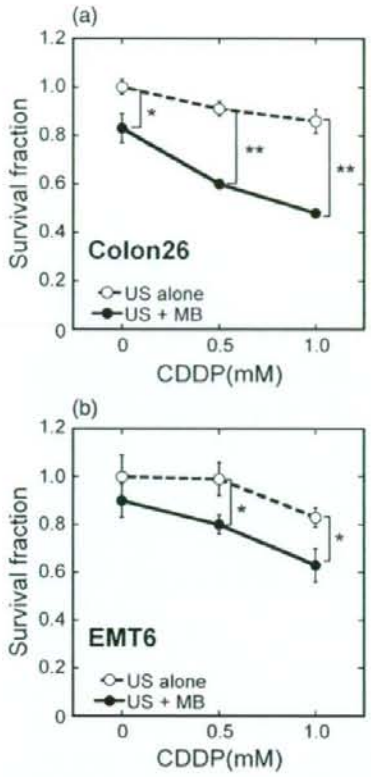

Fig. 2. Potentiation of in vitro cis-diamminedichloroplatinum (II) (CDDP) cytotoxicity in Colon 26 and EMT6 cells. (a) Colon 26: (s) ultrasound (US) alone (n = 5) and (d) US + microbubbles (MB) (n = 5). (b) EMT6: (s) US alone (n = 5) and (d) US + MB (n = 5). Cell survival was measured by a 3-(4,5-dimethylthiazol-2-yl)-2, 5-diphenyltetrazolium bromide (MTT) assay 24 h after US exposure. US intensity 0.5 W/cm2; duty cycle 50%; number of pulses 2000; pulse repletion frequency 250 Hz; and exposure time 10 s. The bars represent mean ± SEM. *P < 0.05, **P < 0.01.

Cytotoxicity *in vitro*. The cytotoxicity of various doses of CDDP in the presence of US with and without MB was tested on Colon 26 and EMT6 cells (Fig. 2). A marked increase in CDDP toxicity was observed under the US–MB conditions, whereas US alone did not significantly affect cell survival with various CDDP concentrations. The CDDP toxicity depended slightly on the cell type.

Apoptosis assay. CDDP is known to induce apoptosis.[25] We confirmed the involvement of apoptosis in mediating cytotoxicity in response to CDDP. Cells undergoing apoptosis demonstrate characteristic nuclear morphological changes with DAPI staining. Figure 3 shows phase contrast and DAPI images of Colon 26 cells. Untreated control cells (Fig. 3a,b) and cells treated with US + MB (Fig. 3c,d), CDDP alone (Fig. 3e,f), and CDDP + US (Fig. 3g,h) showed extremely little condensed or fragmented chromatin. The majority of cells treated with CDDP + US + MB (Fig. 3i,j) displayed apoptotic features, including condensed nuclei and nuclear fragmentation.

Induction of caspase-3 has been suggested as a marker of apoptosis.[26] Figure 4 shows that treatment with US + MB activates caspase-3 as compared to treatment with CDDP alone or with CDDP + US. The caspase activity increases with time. Taken together, the data presented in Figures 3 and 4 demonstrate that the CDDP + US + MB combination decreases cell viability and that this reduction in cell survival is associated with increased induction of apoptosis. In the present study, we did not consider the activation of caspase-3 by US because US alone did not contribute to the survival fraction (Fig. 2) and subsequent apoptosis induction (Fig. 3).

***In vivo* therapeutic effects of MB.** From the above *in vitro* experiments, we found that MB associated with US are able to trigger the uptake of small molecules (Fig. 1), thereby inducing antitumor effects (Fig. 2) and apoptosis (Figs 3,4) in conjunction with CDDP. Thereafter, we investigated the *in vivo* antitumor effects of using MB, in cases in which the xenografts of HT29-luc cells were used. We investigated the antitumor effects of CDDP + US + MB on the xenografts with two different CDDP concentrations (0.5 and 1.25 μg/g bodyweight) on days 4, 7, 9, and 11. The luciferase activity for each concentration of CDDP + US + MB was normalized with each concentration of CDDP + US that was administered previously (Fig. 5a) in order to determine the antitumor effects of MB alone. The activities of the MB were recognized after day 7 (second treatment) in both groups. On day 11, a significant reduction was observed in the CDDP + US + MB group compared to the control and US + MB

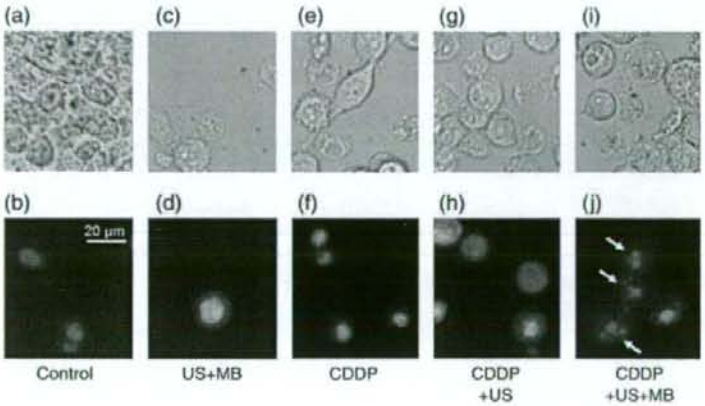

Fig. 3. Nuclear condensation and fragmentation. (a,c,e,g,i) Differential interference contrast and (b,d,f,h,j) 4′,6-diamidino-2-phenylindole (DAPI) fluorescence images of representative viable Colon 26 cells 24 h after treatment. 10 μmol/L cis-diamminedichloroplatinum (II) (CDDP): (a,b) control, (c,d) ultrasound (US) + microbubbles (MB), (e,f) CDDP, (g,h) CDDP + US, and (i,j) CDDP + US + MB. Round or shrunken nuclei of DAPI-stained cells (white arrows) are hallmarks of apoptosis in (j). Experiments were repeated three times with similar results. Scale bar = 20 μm. Ultrasound intensity 1.0 W/cm^2; duty cycle 50%; number of pulses 2000; pulse repletion frequency 250 Hz; and exposure time 10 s.

doi: 10.1111/j.1349-7006.2008.00989.x

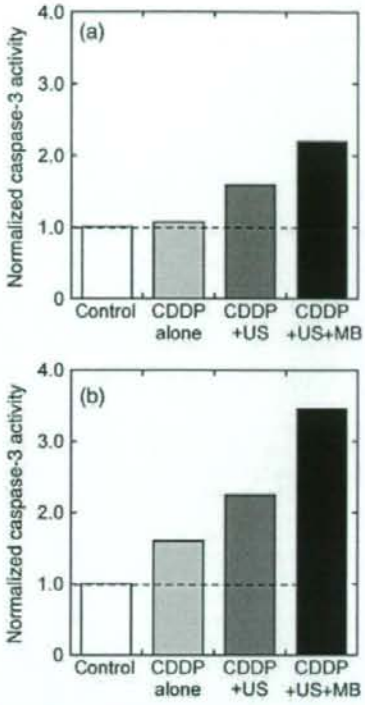

Fig. 4. Upregulation of the proapoptotic gene caspase-3. Colon 26 cells were treated with cis-diamminedichloroplatinum (II) (CDDP) (10 μmol/L) in the presence of ultrasound (US) with and without microbubbles (MB). Caspase-3 activity was measured at 24 h after treatment. Twelve wells from 48-well plates were analyzed for each condition. Results are expressed as the number of molecules of p-nitroaniline (pNA) (nmol) released by 1 mg of protein in (a) 1 and (b) 2 h. Ultrasound intensity 1.0 W/cm²; duty cycle 50%; number of pulses 2000; pulse repletion frequency 250 Hz; and exposure time 10 s.

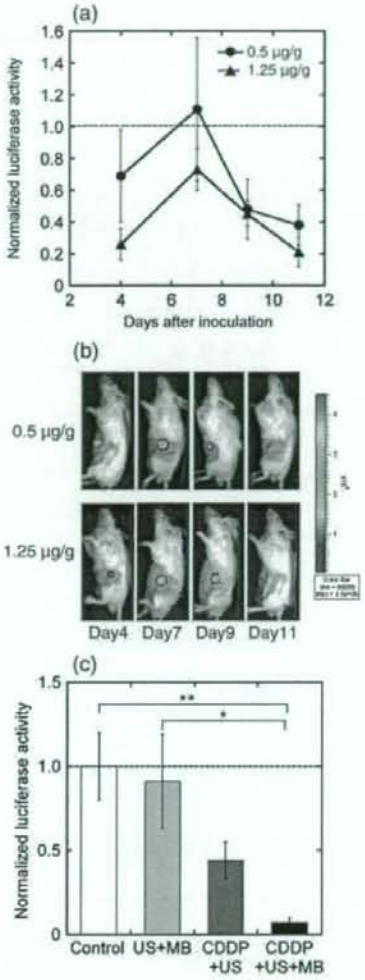

Fig. 5. Antitumor effects of cis-diamminedichloroplatinum (II) (CDDP) + ultrasound (US) + microbubbles (MB) on HT29-luc xenografts with two different CDDP concentrations (0.5 and 1.25 μg/g bodyweight) on days 4, 7, 9, and 11. Ultrasound intensity 3.0 W/cm²; duty cycle 20%; number of pulses 200; pulse repletion frequency 1000 Hz; and exposure time 60 s. Luciferase activity after (a) treatment and (b) bioluminescence imaging. The luciferase activity under each concentration of CDDP + US + MB was normalized with each concentration of CDDP + US. CDDP (0.5 μg/g bodyweight) + US ($n = 4$), CDDP (0.5 μg/g bodyweight) + US + MB ($n = 4$), CDDP (1.25 μg/g bodyweight) + US ($n = 4$), CDDP (1.25 μg/g bodyweight) + US + MB ($n = 4$). (c) The luciferase activity normalized with that of control at day 11, where the concentration of CDDP was 1.25 μg/g bodyweight. Control ($n = 5$), US + MB ($n = 4$). The bars represent mean ± SEM. $^*P < 0.05$, $^{**}P < 0.01$.

groups. These effects were recognized by bioluminescence images (Fig. 5b). Figure 5c shows antitumor effects for different conditions (US + MB, CDDP + US, CDDP + US + MB) at day 11, where the CDDP concentration was 1.25 μg/g bodyweight, and the bioluminescence of each condition was normalized with that of the control at day 11. There was no significant difference between control and US + MB. CDDP alone was recognized as the difference between US + MB and CDDP + US, where CDDP alone decreased US + MB by 48.4%. MB further reduced CDDP + US by 84.1%.

Discussion

The US–MB method permeabilizes the cell membrane directly, thereby allowing the delivery of exogenous molecules into the cells. Electroporation is also a method that is used to permeabilize the cell membrane by direct application of an external electric field. Cemazar *et al.* delivered CDDP into both murine sarcoma cisplatin-sensitive TBL.C12 cells and their resistant subclones, namely, TBL.C12.Pt cells.[27] These cells were treated *in vivo* by electroporation, and their platinum content was measured by atomic absorption. Based on their findings, the authors suggested that 10^6 platinum molecules were delivered into TBL.C12 and TBL.C12.Pt cells at 0.05 and 0.46 μg/mL, respectively, where these concentrations correspond to the 50% inhibitory concentration values of platinum for these cells. Our finding that 10^6–10^7 calcein molecules were internalized per cell at 200 μmol/L, as shown in Figure 1a, is in agreement with the finding of Cemazar *et al.* and demonstrates that US–MB permeabilization is as efficient as electroporation in the permeabilization of cell membranes.

There are several anticancer drugs with a similar molecular weight to CDDP. For example, the molecular weight of vincristine is 923, and that of taxol is 854. There is not even one order difference between these molecules and cisplatin, which has a molecular weight of 300. Therefore, we think that the same number of molecules will be delivered into cells by this method. However, it is noted that the number of molecules internalized is not directly correlated with subsequent antitumor effects.

Following the application of MB and US, the cell membrane surface becomes rough and is characterized by depressions that are reversible within 24 h after US exposure.[28,29] Collapsed MB or cavitation bubbles generated by collapsed MB induce impulsive pressures such as liquid jets and shock waves; these pressures affect the neighboring cells. The shock wave propagation distance from the center of a cavitation bubble that has the potential to damage the cell membrane is considerably larger than the maximum radius of the cavitation bubble.[8] Molecular dynamic simulation has revealed that the cell membrane affected by the shock wave is deformed, thereby allowing the entry of exogenous molecules into the cells.[30] Although the membrane permeabilization time has not been measured accurately, it has been reported that the membrane reseals within 80 s when it is permeabilized by shock waves.[31] When 1176 water molecules are delivered into a lipid bilayer comprising 128 dipalmitoylphosphatidylcholine molecules, a water pore of 1.9-nm diameter is formed in the lipid bilayer;[30] this water pore is larger than the CDDP with a diameter of 0.48 nm.

As shown in Figure 1, the US–MB method enhances cell permeability, thereby allowing the delivery of a large number of CDDP molecules into the cells. The combination of high-intensity ultrasound (shock waves) and generated cavitation bubbles – the same concept as that used in the US–MB method – can deliver CDDP molecules into the cells.[32-35] However, the cytotoxicity of CDDP depends on the cell type (Fig. 2); therefore, resistance to CDDP is not completely overcome simply by the application of US and MB (or cavitation bubbles).

The delivery of CDDP into cells induces apoptosis.[36] Apoptotic pathways involved in mediating CDDP-induced cellular effects have been investigated thoroughly.[37] The apoptotic induction resulting from CDDP delivery was confirmed by DAPI staining (Fig. 3) and measurement of caspase-3 activity (Fig. 4). The upregulation of caspase-3 coincides with the observations of previous reports.[10,11,38,39] Caspase-3 is a key effector of apoptosis that is responsible for the proteolytic cleavage of cytoskeletal proteins, kinase, and DNA repair enzymes.[40] The signaling pathway that mediates US-induced apoptosis has been investigated previously.[11,41]

In the *in vivo* experiments, CDDP and MB were injected intratumorally on days 3, 7, and 10 after the injection with tumor cells (HT29-luc), and the tumor was exposed to US. The normalized luciferase activity increased by day 7 and decreased afterwards. This indicates that the antitumor effects resulted from the activity of MB becoming dominant against the tumorigenesity. Tumor growth was suppressed effectively, indicating that the US–MB method provides a synergistic effect with antitumor drugs.[42,43]

We used a local administration system in the *in vivo* experiments (direct injection of CDDP + MB and local US exposure). This local exposure to US has more advantages than the currently available local therapies such as surgery and radiotherapy. However, the usefulness of local therapy is expected to be limited to a particular tumor or a particular tumor stage. For example, hepatocellular carcinomas and brain gliomas seldom metastasize to other organs. Instead, hepatocellular carcinomas and gliomas grow within the liver and brain, respectively, and eventually cause death without metastasizing to other organs. Because these tumors are fed by a tumor-feeding artery, the arterial injection of any anticancer agent (ACA) into the tumor-feeding artery is the most direct way of delivering it into the tumors, mainly because of the first-path effect. With regard to superficial bladder cancer recurrences, half of all such cases recur, and 10–30% progress to a higher grade or stage and form local invasive cancer. Intravesical administration of ACA is known to prolong the duration of progression-free survival. For a clinically randomized phase III trial conducted in patients with stage III ovarian cancer, local intraperitoneal injection of ACA can prolong the duration of overall survival, compared to systemic intravenous injection.[44]

According to the above mentioned evidence, we believe that it is possible to establish a local ACA delivery system in experimental animal models in anticipation of future clinical trials. The US–MB method has the advantages of tissue specificity and non-invasiveness. In addition, this method can be applied repeatedly to patients without immunogenicity.[21] However, the efficiency of molecular delivery into cells is low, and the subsequent bioeffects are not adequate to be investigated by clinical trials. Recently, many types of MB with characteristics of tissue specificity and drug incorporation have been developed[45] and the US exposure conditions have been investigated.[46,47] Combination of the US–MB method with other physical methods such as hyperthermia has also been investigated.[48] In our laboratory, we have investigated the relationship between the physicochemical properties (zeta potential, size, and lipid components) of MB and the transfection efficiency (data not shown).

In conclusion, in the present study we have demonstrated that the US–MB method combined with the well-known chemotherapeutic agent CDDP has great therapeutic potential in cancer therapy. By reducing the dose of CDDP required to induce cell death through the abovementioned method it may be possible to increase the therapeutic action of the drug and to limit the toxicity of the treatment.

Acknowledgments

We thank Fuki Oosawa for her technical assistance. S.M. acknowledges Grant-in-Aid for Scientific Research (B) (19390507) and H.M. acknowledges Grant-in-Aid for Scientific Research (B) (19592334). G.V. acknowledges the program and projects grants from Cancer Research, UK, Institut national de la santé et de la recherche médicale (INSERM), Ligue Contre le Cancer and support through grant 0607-3D1615–66/AO INSERM from the French National Cancer Institute. T.K. acknowledges Grant-in-Aid for Scientific Research (B) (20300173), and Grant-in-Aid for Scientific Research on Priority Area MEXT (20015005). Y.M. and T.K. acknowledge Grant for Research on Nanotechnical Medical, the Ministry of Health, Labour, and Welfare of Japan (H19-nano-010). G.V. and T.K. acknowledge the Japan–France Integrated Action Program Joint Project. CDDP was donated by Nihon Kayaku (Tokyo, Japan).

References

1 Klibanov AL. Ligand-carrying gas-filled microbubbles: ultrasound contrast agents for targeted molecular imaging. *Bioconjug Chem* 2005; **16**: 9–17.

2 Harvey CJ, Blomley MJ, Eckersley RJ, Cosgrove DO. Developments in ultrasound contrast media. *Eur Radiol* 2001; **11**: 675–89.

3 Barak M, Katz Y. Microbubbles: pathophysiology and clinical implications. *Chest* 2005; **128**: 2918–32.

4 Lindner JR. Molecular imaging with contrast ultrasound and targeted microbubbles. *J Nucl Cardiol* 2004; **11**: 215–21.

5 Chen WS, Matula TJ, Crum LA. The disappearance of ultrasound contrast bubbles: observations of bubble dissolution and cavitation nucleation. *Ultrasound Med Biol* 2002; **28**: 793–803.

doi: 10.1111/j.1349-7006.2008.00989.x

6 Miller DL, Dou C. Membrane damage thresholds for 1- to 10-MHz pulsed ultrasound exposure of phagocytic cells loaded with contrast agent gas bodies *in vitro*. *Ultrasound Med Biol* 2004; **30**: 973–7.
7 Hallow DM, Mahajan AD, McCutchen TE, Prausnitz MR. Measurement and correlation of acoustic cavitation with cellular bioeffects. *Ultrasound Med Biol* 2006; **32**: 1111–22.
8 Kodama T, Tomita Y, Koshiyama K, Blomley MJ. Transfection effect of microbubbles on cells in superposed ultrasound waves and behavior of cavitation bubble. *Ultrasound Med Biol* 2006; **32**: 905–14.
9 Feril LB Jr, Tsuda Y, Kondo T *et al*. Ultrasound-induced killing of monocytic U937 cells enhanced by 2,2'-azobis (2-amidinopropane) dihydrochloride. *Cancer Sci* 2004; **95**: 181–5.
10 Firestein F, Rozenszajn LA, Shemesh-Darvish L, Elimelech R, Radnay J, Rosenschein U. Induction of apoptosis by ultrasound application in human malignant lymphoid cells: role of mitochondria–caspase pathway activation. *Ann NY Acad Sci* 2003; **1010**: 163–6.
11 Honda H, Kondo T, Zhao QL, Feril LB Jr, Kitagawa H. Role of intracellular calcium ions and reactive oxygen species in apoptosis induced by ultrasound. *Ultrasound Med Biol* 2004; **30**: 683–92.
12 Chaussy C, Thuroff S, Rebillard X, Gelet A. Technology insight: high-intensity focused ultrasound for urologic cancers. *Nat Clin Pract Urol* 2005; **2**: 191–8.
13 Colombel M, Gelet A. Principles and results of high-intensity focused ultrasound for localized prostate cancer. *Prostate Cancer Prostatic Dis* 2004; **7**: 289–94.
14 Hou CC, Wang W, Huang XR *et al*. Ultrasound–microbubble-mediated gene transfer of inducible Smad7 blocks transforming growth factor-β signaling and fibrosis in rat remnant kidney. *Am J Pathol* 2005; **166**: 761–71.
15 Shimamura M, Sato N, Taniyama Y *et al*. Gene transfer into adult rat spinal cord using naked plasmid DNA and ultrasound microbubbles. *J Gene Med* 2005; **7**: 1468–74.
16 Takahashi M, Kido K, Aoi A, Furukawa H, Ono M, Kodama T. Spinal gene transfer using ultrasound and microbubbles. *J Control Release* 2007; **117**: 267–72.
17 Gambihler S, Delius M, Ellwart JW. Permeabilization of the plasma membrane of L1210 mouse leukemia cells using lithotripter shock waves. *J Membr Biol* 1994; **141**: 267–75.
18 Kodama T, Doukas AG, Hamblin MR. Shock wave-mediated molecular delivery into cells. *Biochim Biophys Acta* 2002; **1542**: 186–94.
19 Boulikas T, Vougiouka M. Cisplatin and platinum drugs at the molecular level. *Oncol Reports* 2003; **10**: 1663–82.
20 Tennant JR. Evaluation of the trypan blue technique for determination of cell viability. *Transplantation* 1964; **2**: 685–94.
21 Aoi A, Watanabe Y, Mori S, Takahashi M, Vassaux G, Kodama T. Herpes simplex virus thymidine kinase-mediated suicide gene therapy using nano/microbubbles and ultrasound. *Ultrasound Med Biol* 2008; **34**: 425–34.
22 Kodama T, Doukas AG, Hamblin MR. Delivery of ribosome-inactivating protein toxin into cancer cells with shock waves. *Cancer Lett* 2003; **189**: 69–75.
23 Kodama T, Hamblin MR, Doukas AG. Cytoplasmic molecular delivery with shock waves: importance of impulse. *Biophys J* 2000; **79**: 1821–32.
24 Kodama T, Tan PH, Offiah I *et al*. Delivery of oligodeoxynucleotides into human saphenous veins and the adjunct effect of ultrasound and microbubbles. *Ultrasound Med Biol* 2005; **31**: 1683–91.
25 Kojima H, Endo K, Moriyama H *et al*. Abrogation of mitochondrial cytochrome *c* release and caspase-3 activation in acquired multidrug resistance. *J Biol Chem* 1998; **273**: 16 647–50.
26 Abraham MC, Shaham S. Death without caspases, caspases without death. *Trends Cell Biol* 2004; **14**: 184–93.
27 Cemazar M, Miklavcic D, Mir LM *et al*. Electrochemotherapy of tumours resistant to cisplatin: a study in a murine tumour model. *Eur J Cancer* 2001; **37**: 1166–72.
28 Duvshani-Eshet M, Adam D, Machluf M. The effects of albumin-coated microbubbles in DNA delivery mediated by therapeutic ultrasound. *J Control Release* 2006; **112**: 156–66.
29 Taniyama Y, Tachibana K, Hiraoka K *et al*. Local delivery of plasmid DNA into rat carotid artery using ultrasound. *Circulation* 2002; **105**: 1233–9.
30 Koshiyama K, Kodama T, Yano T, Fujikawa S. Structural change in lipid bilayers and water penetration induced by shock waves: molecular dynamics simulations. *Biophys J* 2006; **91**: 2198–205.
31 Lee S, Anderson T, Zhang H, Flotte TJ, Doukas AG. Alteration of cell membrane by stress waves *in vitro*. *Ultrasound Med Biol* 1996; **22**: 1285–93.
32 Barlogie B, Corry PM, Drewinko B. *In vitro* thermochemotherapy of human colon cancer cells with cis-dichlorodiammineplatinum (II) and mitomycin C. *Cancer Res* 1980; **40**: 1165–8.
33 Weiss N, Delius M, Gambihler S, Eichholtz-Wirth H, Dirschedl P, Brendel W. Effect of shock waves and cisplatin on cisplatin-sensitive and – resistant rodent tumors *in vivo*. *Int J Cancer* 1994; **58**: 693–9.
34 Worle K, Steinbach P, Hofstadter F. The combined effects of high-energy shock waves and cytostatic drugs or cytokines on human bladder cancer cells. *Br J Cancer* 1994; **69**: 58–65.
35 Kambe M, Ioritani N, Shirai S *et al*. Enhancement of chemotherapeutic effects with focused shock waves: extracorporeal shock wave chemotherapy (ESWC). *In Vivo* 1996; **10**: 369–75.
36 Yu T, Huang X, Jiang S, Hu K, Kong B, Wang Z. Ultrastructure alterations in adriamycin-resistant and cisplatin-resistant human ovarian cancer cell lines exposed to nonlethal ultrasound. *Int J Gynecol Cancer* 2005; **15**: 462–7.
37 Siddik ZH. Cisplatin: mode of cytotoxic action and molecular basis of resistance. *Oncogene* 2003; **22**: 7265–79.
38 Honda H, Zhao QL, Kondo T. Effects of dissolved gases and an echo contrast agent on apoptosis induced by ultrasound and its mechanism via the mitochondria–caspase pathway. *Ultrasound Med Biol* 2002; **28**: 673–82.
39 Lagneaux L, de Meulenaer EC, Delforge A *et al*. Ultrasonic low-energy treatment: a novel approach to induce apoptosis in human leukemic cells. *Exp Hematol* 2002; **30**: 1293–301.
40 Li Y, Cohen R. Caspase inhibitors and myocardial apoptosis. *Int Anesthesiol Clin* 2005; **43**: 77–89.
41 Abdollahi A, Domhan S, Jenne JW *et al*. Apoptosis signals in lymphoblasts induced by focused ultrasound. *FASEB J* 2004; **18**: 1413–14.
42 Haag P, Frauscher F, Gradl J *et al*. Microbubble-enhanced ultrasound to deliver an antisense oligodeoxynucleotide targeting the human androgen receptor into prostate tumours. *J Steroid Biochem Mol Biol* 2006; **102**: 103–13.
43 Bekeredjian R, Kuecherer HF, Kroll RD, Katus HA, Hardt SE. Ultrasound-targeted microbubble destruction augments protein delivery into testes. *Urology* 2007; **69**: 386–9.
44 Armstrong DK, Bundy B, Wenzel L *et al*. Intraperitoneal cisplatin and paclitaxel in ovarian cancer. *N Engl J Med* 2006; **354**: 34–43.
45 Suzuki R, Takizawa T, Negishi Y *et al*. Gene delivery by combination of novel liposomal bubbles with perfluoropropane and ultrasound. *J Control Release* 2007; **117**: 130–6.
46 Tartis MS, McCallan J, Lum AF *et al*. Therapeutic effects of paclitaxel-containing ultrasound contrast agents. *Ultrasound Med Biol* 2006; **32**: 1771–80.
47 Rychak JJ, Klibanov AL, Hossack JA. Acoustic radiation force enhances targeted delivery of ultrasound contrast microbubbles: *in vitro* verification. *IEEE Trans Ultrason Ferroelectr Freq Control* 2005; **52**: 421–33.
48 Feril LB Jr, Kondo T. Biological effects of low intensity ultrasound: the mechanism involved, and its implications on therapy and on biosafety of ultrasound. *J Radiat Res (Tokyo)* 2004; **45**: 479–89.

Prostaglandins, Leukotrienes and Essential Fatty Acids 79 (2008) 21–26

Contents lists available at ScienceDirect

Prostaglandins, Leukotrienes and Essential Fatty Acids

journal homepage: www.elsevier.com/locate/plefa

Fatty acid-binding protein regulates LPS-induced TNF-α production in mast cells

Noriko Yamamoto [a,b,1], Izumi Kaneko [c,1], Keiju Motohashi [a,e], Hiroyuki Sakagami [d], Yasuhiro Adachi [a], Nobuko Tokuda [a], Tomoo Sawada [a], Hiroshi Furukawa [c], Yoshiya Ueyama [b], Kohji Fukunaga [e], Masao Ono [c], Hisatake Kondo [d], Yuji Owada [a,*]

[a] Department of Organ Anatomy, Yamaguchi University Graduate School of Medicine, 1-1-1 Minami Kogushi, Ube 755-8505, Japan
[b] Department of Oral and Maxillofacial Surgery, Yamaguchi University Graduate School of Medicine, Japan
[c] Department of Pathology, Tohoku University Graduate School of Medicine, Japan
[d] Department of Histology, Tohoku University Graduate School of Medicine, Japan
[e] Department of Pharmacology, Tohoku University Graduate School of Pharmaceutical Science, Japan

ARTICLE INFO

Article history:
Received 22 February 2008
Received in revised form
30 May 2008
Accepted 28 June 2008

ABSTRACT

There has been increasing evidence for the involvement of fatty acid-binding proteins (FABPs) in the cytokine production of macrophages and dendritic cells probably through the control of cellular lipid metabolism and signal transduction. Since mast cells (MCs) are recently shown to be involved in immune response through modification of cytokine production, it is possible that some FABPs could also be involved in the immune response of MCs. In this study, we found that epidermal-type FABP (E-FABP) was expressed in murine bone marrow-derived MCs (BMMCs). Using BMMCs from genetically E-FABP-null mutated mice, we demonstrated that E-FABP in BMMCs plays a key role in the production of TNF-α following lipopolysaccharide (LPS) stimulation. In the *in vivo* septic peritonitis model (cecal ligation and puncture model), E-FABP-null mice showed a significantly increased mortality compared to wild-type mice. However, no significant difference in antigen-induced cytokine production was observed between wild-type and E-FABP-null BMMCs, and systemic anaphylaxis was equally induced *in vivo* in both wild-type and E-FABP-null mice. These results suggest that E-FABP is specifically involved in the LPS-induced cytokine production of MCs, and could play a role in the host-defense against bacterial infection, possibly through regulation of TNF-α production.

1. Introduction

Mast cells (MCs) induce profound allergic responses through release of a variety of inflammatory mediators, including histamine and a number of immuno-regulatory cytokines, by cross-linking high-affinity receptors for IgE (FcεRI) on their plasma membrane and appropriate antigens [1,2]. In contrast to the harmful role of MCs, recent studies have revealed that MCs that reside in high numbers at the host–environment interface play a protective role in the host defense against bacteria [3,4]. When MCs are exposed to lipopolysaccharide (LPS), a bacterial cell wall component from gram-negative bacteria, they produce proinflammatory cytokines such as TNF-α and IL-6 through activation of toll-like receptors (TLRs) on their cell surface [5,6]. This cytokine response of MCs to various pathogens is strictly regulated by the cellular chemical environments including eicosanoids such as leukotrienes (LTs) and prostaglandins (PGs) [7–10], derivatives from long-chain fatty acids (LCFA). Thus, LCFAs are supposed to directly modulate the inflammatory response through modulation of intracellular signal transduction pathways of MCs [11]. However, the molecular mechanism underlying such regulation by LCFAs is still poorly understood.

Due to the hydrophobic property of LCFAs, intracellular transport or storage of LCFAs requires an interaction with carrier proteins such as fatty acid-binding proteins (FABPs) [12]. FABPs constitute a multigene family of structurally homologous cytosolic proteins capable of binding LCFAs and various eicosanoids, and could work as vehicles of water-insoluble ligands. Recent evidence suggests that the FABP family of proteins could play a role in (i) prompting cellular flux of poorly water-soluble ligands and their subsequent metabolic utilization or transformation, (ii) sequestration of ligands that limits their association with alternative-binding sites in the cell, and (iii) transport of ligands in

* Corresponding author. Tel.: +81 836 22 2201; fax: +81 836 22 2203.
E-mail address: yowada@yamaguchi-u.ac.jp (Y. Owada).
[1] N.Y. and I.K. contributed equally to this work.

0952-3278/$ - see front matter © 2008 Elsevier Ltd. All rights reserved.
doi:10.1016/j.plefa.2008.06.003

a manner that promotes their association with alternative-binding sites in the cell [13]. Among members of the FABP family, epidermal-type FABP (E-FABP), also called mal1, KLBP, fabp5 or C-FABP, is expressed not only in keratinocytes [14,15] but also in macrophages and dendritic cells (DCs), which are known to be involved in inflammatory response [16–18]. The present authors have revealed that E-FABP-null splenic DCs show an increased production of IL-12 in response to LPS, suggesting a role of E-FABP as a modulator of cytokine production in the immune cells [19,20]. These findings suggest the possibility that FABP may also be involved in inflammatory response mediated by MCs through regulation of MC cytokine production. Here, we show that E-FABP, which is specifically expressed in MCs, modulates MC response to bacteria through regulation of TNF-α production.

2. Materials and methods

2.1. Animals

The generation of E-FABP gene knockout mice was described previously [21]. Mice used in this study were backcrossed from a mixed 129SVJ × C57BL/6 background onto the C57BL/6 for at least eight generations and were intercrossed to produce wild-type and E-FABP-null mice. All experimental protocols were reviewed by the committee on the ethics of animal experiments of Yamaguchi University.

2.2. Preparations of BMMCs

Bone marrow-derived MCs (BMMCs) were isolated from the bone marrow of wild-type and E-FABP-null mutant mice on postnatal 12 week as previously described [22]. Briefly, mice were sacrificed, and intact femurs and tibias were removed. Sterile endotoxin-free medium was repeatedly flushed through the bone shaft using needles and syringes, and the bone marrow cells were passed through a nylon mesh to remove the bone fragments. The cell suspension was centrifuged at 320 × *g* for 20 min at 4 °C and cultured at a concentration of 0.5–1 × 10^6 nucleated cells/ml in RPMI 1640 supplemented with 10% FCS, 100 U/ml penicillin, 100 μg/ml streptomycin, 1 mM sodium pyruvate, 1 × non-essential amino acid, 50 μM 2-mercaptoethanol, and 5 ng/ml murine IL-3 (R&D Systems, St. Louis, MO, USA). The medium was replaced three times a week with the fresh complete medium.

BMMCs were monitored for purity after 4 weeks by flow cytometry (FACS Caliber, Becton Dickinson, San Jose, CA, USA). The cells were incubated with fluorescently labeled antibodies in 5% FCS in PBS and were analyzed with CELLQuest Software. BMMCs were identified as double-positive cells for FITC-conjugated anti-IgE and PE-conjugated anti-c-Kit (BD Bioscience Pharmingen, San Diego, CA, USA). After 4 weeks of culture of BMMCs, more than 95% of the cells were identified as BMMCs (data not shown), and no significant differences were observed between wild-type and E-FABP-null BMMCs in the expression of these two markers (data not shown). Furthermore, no significant differences were detected in the increase of BMMC population during the time course of culture between wild-type and E-FABP-null mice (data not shown).

2.3. Immunocytochemistry

Immunocytochemistry was performed as described previously with slight modification [19]. Briefly, BMMCs were attached onto glass slides using a centrifugal cell collector (TOMY SEIKO, Tokyo, Japan). The cells on glass slides were incubated with a rabbit anti-rat antibody against E-FABP [21] at a concentration of 0.5 μg/ml for 12 h at 4 °C. After incubation with the primary antibody, the cells were incubated with an anti-rabbit antibody labeled by Alexa488 (Invitrogen, Carlsbad, CA, USA). After nuclear-counter staining with DAPI (4′,6,-diamidino-2-phenylindole), the cells were covered with Gel/Mount (Biomeda, Foster City, CA, USA), and observed by confocal laser microscope (LSM5 Pascal; Carl Zeiss, Oberkochen, Germany).

2.4. Immunoblotting

Cells were lysed in a lysis buffer solution that consisted of 12.5 mM Tris–HCl (pH 6.8), 4% SDS, 20% glycerin, 0.01% broomophenol blue, 1 mM PMSF, 1 mM Na_3VO_4, and protease inhibitor cocktail tablet (Roche, Basel, Switzerland). Lysates were cleared by centrifugation at 15,000 rpm for 5 min and boiled in a sample buffer solution. Cell lysates (10 μg of total protein from BMMCs or tissues) were loaded onto 10% SDS–PAGE, fractionated and transferred to PVDF membranes (Osmonic Inc., Livemore, CA, USA). After blocking with 5% normal goat serum, the membrane was incubated with an appropriate primary antibody. Primary antibodies used in the present study were anti-rat E-FABP antibody [21], anti-mouse B (brain type)—FABP antibody [23], anti-mouse L (liver type)—FABP antibody [24], anti-mouse H (heart type)—FABP antibody [25] and anti-mouse A (adipocyte type)—FABP antibody [26]. After incubation with the primary antibody, the membranes were subsequently incubated with the anti-rabbit secondary antibody conjugated with HRP (Sigma, St. Louis, MO, USA). The immunopositive bands were visualized with the enhanced chemiluminescence immunoblotting detection system (Amersham Bioscience, Buckinghamshire, UK), and the images were digitally captured by ChemiDoc XRS (Bio-Rad Laboratories, Hercules, CA, USA).

2.5. Activation of BMMCs

BMMCs were seeded at 1 × 10^6 cells per well in 96-well plates. For antigen stimulation, BMMCs were sensitized overnight with 1 μg/ml trinitrophenyl (TNP) hapten-specific IgE (TNP-IgE) and 1 ng/ml TNP-conjugated ovalbumin (TNP-OVA) (fraction VII; Sigma). For LPS stimulation, BMMCs were stimulated by LPS (*E. coli* 055:B5, Sigma) at a dose of 0.1 μg/ml. For application of fatty acids together with LPS, a given fatty acid was mixed with RPMI medium for 30 min to allow binding of the fatty acid with fatty acid free-albumin (Sigma) prior to addition to BMMCs at indicated concentrations.

2.6. Determination of cytokine production by ELISA

Cell supernatants after 24 h of LPS or IgE+OVA sitimulation were collected, and used for cytokine measurement by ELISA. Commercially available ELISA kits (BD OptEIA Set; BD Biosciences Pharmingen, San Diego, CA, USA) were used for measuring the concentration of TNF-α and IL-6 in supernatant fraction samples of the cell culture according to the manufacture's manual.

2.7. RT-PCR

Total RNAs were isolated from BMMCs at 30 min after LPS stimulation using TRIzol solution (GIBCO-BRL, Burlington, ON, Canada). The detail of semi-quantitative RT-PCR was described elsewhere [20]. First-strand cDNA was synthesized using a reverse transcription system (Promega, Madison, WI, USA). PCR was carried out with following primers: β-actin: 5′-CAGGAGAT-GGCCACTGCCGCA and 5′-CTCCTTCTGCATCCTGTCAGCA; TNF-α:

5′-CTGGGACAGTGACCTGGACT and 5′-GCACCTCAGGGAAGAGTCTG; IL-6: 5′-GAAATGAGAAAAGAGTTGTGC and 5′-ATTGGAAATTGGGGTAGGAAG.

2.8. Cecal ligation and puncture (CLP)

CLP were performed as previously described by others with slight modification [3,27]. In brief, mice were anesthetized by i.p. injection of 50 mg/kg sodium pentobarbital. A 1-cm midline incision on the anterior abdominal wall was made. The cecum was exposed and filled with feces by squeezing stool gently back from the ascending colon. The cecum was 50% ligated below the ileocecal valve and then punctured using a 21 G needle followed by gentle squeezing of the cecum. Mice were observed for mortality at least five times daily over a period of 10 days. Before CLP was performed, the mice were coded so that the CLP was done without identifying individual groups.

2.9. Passive anaphylactic response

For IgE-mediated systemic anaphylaxis, 10 weeks-old male mice were used ($n = 6$ from each genotype). Mice were intravenously injected with TNP-IgE (125 μg per mouse dissolved with 200 μl of saline). After 24 h, TNP-OVA (1 mg per mouse dissolved with 200 μl of saline) was intravenously injected, and the body temperature were monitored with a rectal thermometer (Shibaura Electronics Co. Ltd., Saitama, Japan) for mice without general anesthesia at 0, 10, 20, 30, 40, 50, 60 and 80 min after the injection.

2.10. Histological quantification of MCs

Tissues including tongue, ear skin and stomach were extirpated from wild-type and E-FABP-null mice, fixed in 10% neutral buffered formalin, and embedded in paraffin. Sections with 4 μm thickness were cut using a sledge microtome (Leica, Wetzler, Germany). Peritoneal lavages were obtained by washing repeatedly the peritoneal cavity with ice-cold PBS, and the smear sections were prepared. After Giemsa staining, the population of MCs in tissues and peritoneal lavages was counted under light microscope. The data were expressed as the number of MCs/mm^2 of tissues.

2.11. Statistical analysis

Data were presented as average ± S.E.M. The survival curve was calculated with the aid of the Kaplan-Meier life-table method and log-rank test using a GraphPad Prism version 4 (GraphPad Software Inc., San Diego, CA, USA). Comparable data were performed using the Student's t-test. Differences were considered statistically at $P < 0.05$.

3. Results

3.1. Identification of E-FABP in the MCs

First, we examined the expression of FABP family members, including A-, B-, E-, H- and L-FABP in the murine BMMCs. As shown in Fig. 1A, E-FABP was expressed in BMMCs and no significant expression of B-, H- and L-FABP was observed in BMMCs. In immmunocytochemical analysis, immunoreactivity for E-FABP was detected in the cytosol as well as nucleus of BMMCs (Fig. 1B). No positive immunoreactivity was detected when

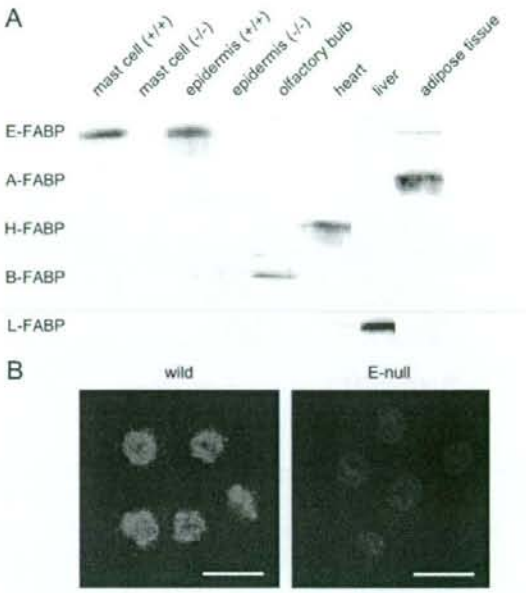

Fig. 1. E-FABP is expressed in mouse BMMCs. (A) Immunoblot analysis of five species of FABPs in BMMCs. Immunopositive single band for E-FABP is detected in BMMCs, while no positive bands for A-, B-, H- or L-FABP are observed. (B) Light micrographs of wild-type and E-FABP-null BMMCs stained with E-FABP antibody (green) and DAPI (blue). Note that E-FABP is localized in the cytoplasmic compartment as well as the nucleus. The bands shown in (A) are obtained from different gels. Bars = 10 μm.

E-FABP antiserum was applied to sections of BMMCs from E-FABP-null mutant mice.

3.2. E-FABP deficiency in BMMCs results in decreased TNF-α and IL-6 production after LPS stimulus

To examine the functional significance of E-FABP in BMMCs, cytokine production in response to LPS- or antigen-stimulation, which is known to be mediated by TLR4 or FcεIR, respectively, was measured in E-FABP-null BMMCs. As shown in Fig. 2, a marked decrease in amount of TNF-α and IL-6 was detected in E-FABP-null BMMCs 24 h after LPS stimulus (Fig. 2A). However, no significant difference in TNF-α and IL-6 was detected between wild-type and E-FABP-null BMMCs when cells were stimulated with a combination of IgE and OVA (Fig. 2B), which is known to be mediated by FcεIR. Gene expression of TNF-α and IL-6 was decreased in E-FABP-null BMMCs 6 h after LPS stimulation when examined by semi-quantitative RT-PCR (Fig. 2D).

3.3. AA enhances cytokine production in BMMCs

E-FABP expression in MCs could mean that LCFAs, which are E-FABP ligands, modulate the immune response in the same way as other immune cells [28]. Thus, we next examined the impact of exogenously applied LCFA on cytokine production of BMMCs after LPS stimuli. As shown in Fig. 2C, AA enhanced production of TNF-α and IL-6 from wild-type and E-FABP-null BMMCs after LPS stimulation in a dose-dependent manner, whereas a combination of IgE and OVA stimulation with each dose of AA examined has no effects (data not shown). Furthermore, no significant changes in production of TNF-α and IL-6 were observed when other fatty

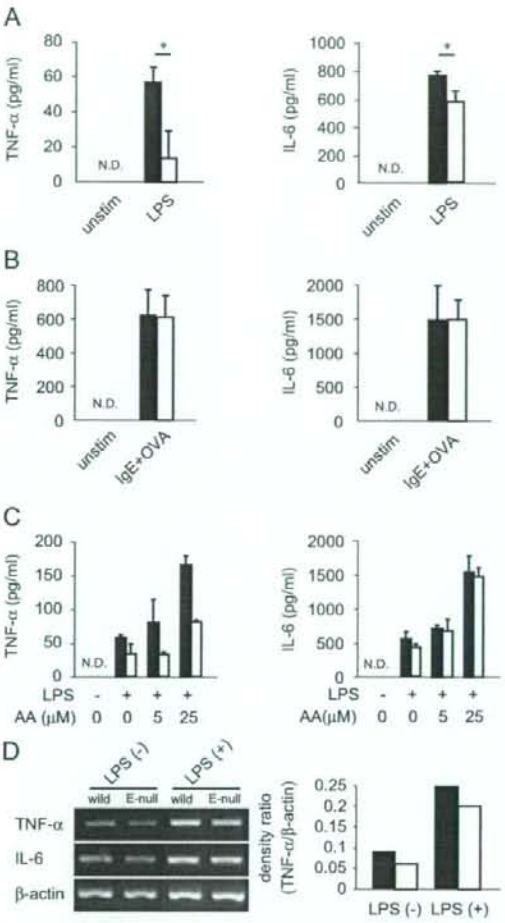

Fig. 2. Decreased production of TNF-α and IL-6 in E-FABP-null BMMCs after LPS stimulation and effect of AA on the production of LPS-induced TNF-α and IL-6. (A) Production of two cytokines after LPS (0.1 μg/ml) stimulation in wild-type and E-FABP-null BMMCs by ELISA. Note a marked decrease of TNF-α and IL-6 in E-FABP-null BMMCs (open column) compared with wild-type (filled column) in the media containing BMMCs 24 h after LPS stimulation. *$P<0.05$. (B) In contrast to (A), note no significant difference in the amount of TNF-α and IL-6 after antigen-stimulation (IgE+OVA) between the two groups. Data are shown as means ± S.E.M. and representative of two independent experiments. (C) LPS (0.1 μg/ml) combined with each dose of AA (0, 5, 25 μM) were added to the culture media containing wild-type (filled column) and E-FABP-null BMMCs (open column). Note that AA enhances LPS-induced production of TNF-α and IL-6 in a dose-dependent manner in BMMCs, but such enhancement of TNF-α by AA was markedly reduced in the E-FABP-null BMMCs especially at a dose of 5 μM AA. Data are shown as means ± S.E.M. and representative of two independent experiments. (D) Expression of mRNA for TNF-α and IL-6 was examined by RT-PCR. A significant decrease of TNF-α mRNA expression is detected in the E-FABP-null BMMCs at 30 min after LPS stimulation. Data are representative of two independent experiments.

acids including palmitic acid, oleic acid, linoleic acid, linolenic acid, stearic acid and docosahexaenoic acid were applied (data not shown). When we examined whether E-FABP deficiency in BMMCs modifies such enhancement of LPS-induced TNF-α or IL-6 production by AA, the induction rate of TNF-α production by AA was significantly decreased in E-FABP-null BMMCs in 5 μM AA application (TNF-α with 5 μM AA/TNF-α without AA = 1.41 in wild versus 0.96 in E-FABP-null BMMCs, $P<0.05$, see Fig. 2C left). However, no impact of E-FABP deficiency was detected in the enhancement of IL-6 production by AA (Fig. 2C right). In addition, we did not observe significant differences between wild-type and E-FABP-null BMMCs in the enhancement of TNF-α production after antigen (IgE-OVA)-stimulation with a combination of various doses of AA incubation (data not shown).

3.4. Lack of E-FABP in MCs leads to increased mortality in a model of acute septic peritonitis

The CLP model was used to evaluate whether decreased TNF-α production after LPS stimulation due to E-FABP deficiency in MCs could affect the MC-mediated host defense against bacteria *in vivo*. As shown in Fig. 3A, E-FABP-null mice showed a significantly increased mortality compared to wild-type mice following CLP.

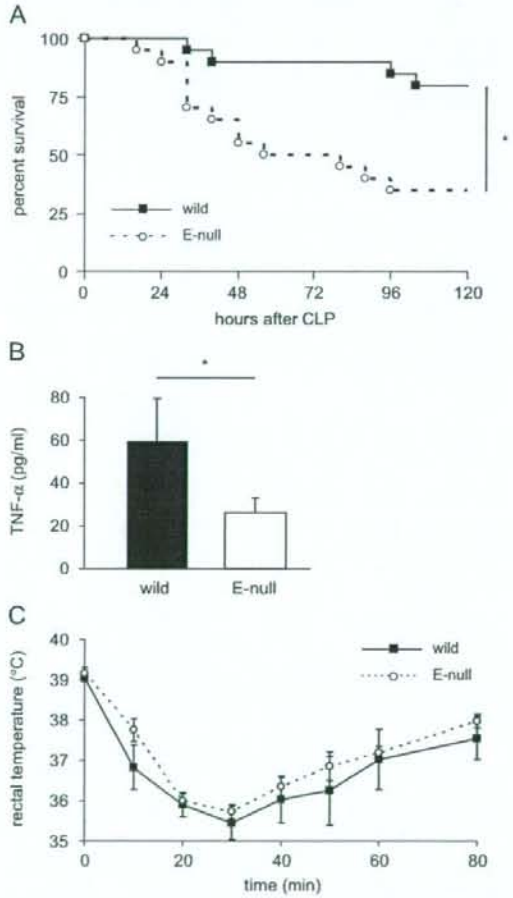

Fig. 3. E-FABP is required for protection of mice from CLP-induced acute septic peritonitis. Wild-type mice and E-FABP-null mice ($n = 25$ per each genotype) were subjected to CLP (cecal ligation and puncture), and the survival rate was monitored. (A) Note a significant increase in the mortality rate of E-FABP-null mice as compared with wild-type mice. (B) Note a decrease in the amount of TNF-α in peritoneal lavage in E-FABP-null mice (open column) as compared with wild-type (filled column) 6 h after CLP. (C) No significant differences in the antigen-induced passive anaphylactic response between wild-type and E-FABP-null mice ($n = 10$ per each genotype) as indicated by rectal temperature after antigen injection. *$P<0.05$. Data are representative of two independent experiments.

Table 1
Populations of tissue-resident MCs are normal in E-FABP-null mice

	Peritoneal cavity ($\times 10^4$ MCs/ml)	Tongue (MCs/mm^2)	Ear skin (MCs/mm^2)	Stomach (MCs/mm^2)
Wild ($n = 5$)	2.6±2.1	48.1±14.6	136.8±17.6	19.5±9.1
E-null ($n = 5$)	3.2±1.7	44.3±7.7	139.4±17.9	17.4±4.2

The number of MCs in wild-type and E-FABP-null were assessed as described in Section 2. Data are shown as means±S.E.M.

Furthermore, the amount of TNF-α in peritoneal lavage 6 h after CLP was significantly decreased in E-FABP-null mice compared with wild-type (Fig. 3B). In order to exclude the possibility that the decreased amount of TNF-α is due to a decreased population density of tissue resident MCs, the population of MCs in various tissues was examined by histological examination, and no significant differences were observed (Table 1). Also, no significant differences were observed between wild-type and E-FABP-null mice in the antigen-induced passive anaphylactic response represented by changes in body temperature after OVA injection (Fig. 3C).

4. Discussion

In the present study, we revealed that E-FABP was solely expressed in mouse BMMCs, and E-FABP gene ablation in BMMCs resulted in a marked decrease of proinflammatory cytokine production after LPS stimulation. The modulatory role of E-FABP in cytokine production in MCs could be specific to LPS because no such decrease of cytokine production was found after antigen (IgE+OVA) stimulation. Furthermore, mice genetically deficient in E-FABP showed a higher mortality rate compared to wild-type mice in the CLP-induced acute septic peritonitis model, which has been shown to reflect LPS-mediated MC function in the innate immunity [3]. Collectively, the present findings suggest that deteriorated protection against acute septic peritonitis in E-FABP-null mice is at least in part due to a decreased production of proinflammatory cytokines including TNF-α in MCs.

Several reports have so far demonstrated the expression and/or possible functions of different FABPs in various immune cells: A-, B-, L- and E-FABPs in monocytes/macrophages [17,29–31], A-FABP in lymphocytes [26] or A- and E-FABPs in DCs [19,20,32]. However, this is the first study about the functional significance of FABP in MCs. LCFAs, cellular ligands of FABP, have been shown to modulate cytokine production after antigen-stimulation in a rat mast cell line [11]. In agreement with these previous results, the present study revealed that exogenously applied AAs enhanced LPS-induced production of TNF-α from BMMCs in a dose-dependent manner. Considering the preferable binding of E-FABP with LCFAs including AA [33], and a possible role of E-FABP as a cellular shuttle of such ligands to various cell organelles such as the nucleus and plasma membrane, it is possible that impaired intracellular transport of AA and/or its bioactive derivatives onto nuclear receptors could occur in E-FABP-null BMMCs. Indeed, in the present study, we detected the elimination of enhancement of TNF-α production by AA in the E-FABP-null BMMCs. However, the further studies are necessary to explain why such elimination of the impact by AA in E-FABP-null BMMCs was observed only in TNF-α but not in IL-6 production.

How the present E-FABP ablation in BMMCs specifically reduced LPS-induced proinflammatory cytokine production remains unclear. It has been shown that the production of inflammatory cytokines by BMMCs is regulated by LPS/TLR4 signaling [5] and/or IgE/FcεRI signaling [34]. The activation of these receptors on MCs is considered to be followed by activation of the NF-κB signaling pathway [5,34]. Recent evidence has suggested that FABPs are involved in the control of intracellular signaling pathways activated by peroxisome proliferators-activated receptors (PPARs) and NF-κB, possibly through regulation of the availability of lipid ligands for these signaling molecules [24,35,36]. In the present study, E-FABP ablation in MCs did not alter the response to antigen-stimulation, suggesting that E-FABP is specifically involved in LPS/TLR4 signaling, but not in IgE/FcεRI signaling. According to previous findings by others, ligand-activated TLR4 recruits cytosolic adaptor molecules that include myeloid differentiation protein 88 (MyD88), MyD88-adaptor like/TIR associated protein (MAL/TIRAP), toll-receptor associated molecule (TRAM). The recruitment of Myd88 by TLR4 results in sequential activation of protein kinase interleukin-1 receptor-associated kinases (IRAKs) and transforming growth factor-β-activated kinase (TAK1). TAK1, in turn, regulates activation of mitogen-activated (MAP) kinases and the transcription factor, NF-κB, with ensuing production of inflammatory cytokines [37]. Thus, it is likely that the alteration of fatty acid metabolism in MCs due to E-FABP ablation may negatively modify the LPS/TLR4-activated signaling pathway at a site upstream of NF-κB, resulting in decreased production of TNF-α and IL-6.

We have recently reported that E-FABP gene ablation in DCs results in enhanced production of IL-12 in response to LPS compared with wild-type DCs. Such an enhancement of IL-12 production in E-FABP-null DCs seems to be contradictory to the present finding that E-FABP-null BMMCs showed a decreased production of TNF-α and IL-6. In this regard, it should be noted that the effect of AA on the production of cytokines in these cells is also opposite: under LPS stimulation, AA enhances TNF-α and IL-6 production in MCs as shown in Fig. 2C but eliminates IL-12 production in DCs [20]. Furthermore, the bioactive AA metabolites such as PGD2, PGE2 and LXA4 are shown to modulate the LPS-activated cytokine production positively in MCs and negatively in DCs, respectively [38,39]. Considering that AA and its bioactive metabolites are cellular ligands of E-FABP, individual E-FABP/ligand complexes may interact with and/or activate discrete molecules and thereby modify the cytokine production differently between MCs and DCs, although the mechanism underlying these different responses to LPS is to be elucidated in the further study.

It has recently been known that FABPs are functionally located at the interface of inflammatory and metabolic systems, and may serve as a subtle-modulator for immune cell responses [40]. We demonstrated in this study that E-FABP-null MCs showed a decreased production of proinflammatory cytokines upon LPS stimulation, leading to a decreased protection against the acute septic peritonitis induced by CLP in mice. This finding suggests that E-FABP in MCs positively regulates the innate immune responses against gram-negative bacteria. Considering various dietary effects of lipids on the immune function and onset of inflammatory diseases [28], and the preferable binding of E-FABP with common dietary LCFAs, the modulation of E-FABP expression in MCs could become a novel therapeutic target in the

regulatory response of MCs against gram-negative bacterial infections.

Acknowledgments

This work was supported by the Grants nos. 19590189 (to Y.O.) and 18390056 (to H.K.) from Japan Society for the Promotion of Science.

References

[1] T.B. Casale, Z. Marom, Mast cells and asthma. The role of mast cell mediators in the pathogenesis of allergic asthma, Ann. Allergy 51 (1983) 2–6.
[2] S.J. Galli, New concepts about the mast cell, N. Engl. J. Med. 328 (1993) 257–265.
[3] B. Echtenacher, D.N. Mannel, L. Hultner, Critical protective role of mast cells in a model of acute septic peritonitis, Nature 381 (1996) 75–77.
[4] J.S. Marshall, Mast-cell responses to pathogens, Nat. Rev. Immunol. 4 (2004) 787–799.
[5] V. Supajatura, H. Ushio, A. Nakao, K. Okumura, C. Ra, H. Ogawa, Protective roles of mast cells against enterobacterial infection are mediated by toll-like receptor 4, J. Immunol. 167 (2001) 2250–2256.
[6] J.S. Marshall, J.D. McCurdy, T. Olynych, Toll-like receptor-mediated activation of mast cells: implications for allergic disease?, Int. Arch. Allergy Immunol. 132 (2003) 87–97.
[7] J.S. Marshall, K. Gomi, M.G. Blennerhassett, J. Bienenstock, Nerve growth factor modifies the expression of inflammatory cytokines by mast cells via a prostanoid-dependent mechanism, J. Immunol. 162 (1999) 4271–4276.
[8] I. Leal-Berumen, P. O'Byrne, A. Gupta, C.D. Richards, J.S. Marshall, Prostanoid enhancement of interleukin-6 production by rat peritoneal mast cells, J. Immunol. 154 (1995) 4759–4767.
[9] C. Feng, E.M. Beller, S. Bagga, J.A. Boyce, Human mast cells express multiple EP receptors for prostaglandin E2 that differentially modulate activation responses, Blood 107 (2006) 3243–3250.
[10] M. Nguyen, M. Solle, L.P. Audoly, et al., Receptors and signaling mechanisms required for prostaglandin E2-mediated regulation of mast cell degranulation and IL-6 production, J. Immunol. 169 (2002) 4586–4593.
[11] N. Nakano, A. Nakao, T. Uchida, et al., Effects of arachidonic acid analogs on FcepsilonRI-mediated activation of mast cells, Biochim. Biophys. Acta 1738 (2005) 19–28.
[12] J.F. Glatz, M.M. Vork, D.P. Cistola, G.J. van der Vusse, Cytoplasmic fatty acid binding protein: significance for intracellular transport of fatty acids and putative role on signal transduction pathways, Prostaglandins Leukot Essent Fatty Acids 48 (1993) 33–41.
[13] N.R. Coe, D.A. Bernlohr, Physiological properties and functions of intracellular fatty acid-binding proteins, Biochim. Biophys. Acta 1391 (1998) 287–306.
[14] P. Madsen, H.H. Rasmussen, H. Leffers, B. Honore, J.E. Celis, Molecular cloning and expression of a novel keratinocyte protein (psoriasis-associated fatty acid-binding protein [PA-FABP]) that is highly up-regulated in psoriatic skin and that shares similarity to fatty acid-binding proteins, J. Invest. Dermatol. 99 (1992) 299–305.
[15] R. Watanabe, H. Fujii, S. Odani, et al., Molecular cloning of a cDNA encoding a novel fatty acid-binding protein from rat skin, Biochem. Biophys. Res. Commun. 200 (1994) 253–259.
[16] Y. Owada, S.A. Abdelwahab, R. Suzuki, et al., Localization of epidermal-type fatty acid binding protein in alveolar macrophages and some alveolar type II epithelial cells in mouse lung, Histochem. J. 33 (2001) 453–457.
[17] M.R. Nourani, Y. Owada, N. Kitanaka, et al., Localization of epidermal-type fatty acid binding protein in macrophages in advanced atretic follicles of adult mice, J. Mol. Histol. 36 (2005) 391–400.
[18] L. Makowski, G.S. Hotamisligil, The role of fatty acid binding proteins in metabolic syndrome and atherosclerosis, Curr. Opin. Lipidol. 16 (2005) 543–548.
[19] N. Kitanaka, Y. Owada, S.A. Abdelwahab, et al., Specific localization of epidermal-type fatty acid binding protein in dendritic cells of splenic white pulp, Histochem. Cell Biol. 120 (2003) 465–473.
[20] N. Kitanaka, Y. Owada, R. Okuyama, et al., Epidermal-type fatty acid binding protein as a negative regulator of IL-12 production in dendritic cells, Biochem. Biophys. Res. Commun. 345 (2006) 459–466.
[21] Y. Owada, H. Takano, H. Yamanaka, et al., Altered water barrier function in epidermal-type fatty acid binding protein-deficient mice, J. Invest. Dermatol. 118 (2002) 430–435.
[22] T. Yuasa, M. Ono, T. Watanabe, T. Takai, Lyn is essential for fcgamma receptor III-mediated systemic anaphylaxis but not for the Arthus reaction, J. Exp. Med. 193 (2001) 563–572.
[23] Y. Owada, S.A. Abdelwahab, N. Kitanaka, et al., Altered emotional behavioral responses in mice lacking brain-type fatty acid-binding protein gene, Eur. J. Neurosci. 24 (2006) 175–187.
[24] C. Wolfrum, C.M. Borrmann, T. Borchers, F. Spener, Fatty acids and hypolipidemic drugs regulate peroxisome proliferator-activated receptors alpha-and gamma-mediated gene expression via liver fatty acid binding protein: a signaling path to the nucleus, Proc. Natl. Acad. Sci. USA 98 (2001) 2323–2328.
[25] F. Guthmann, C. Hohoff, H. Fechner, et al., Expression of fatty-acid-binding proteins in cells involved in lung-specific lipid metabolism, Eur. J. Biochem. 253 (1998) 430–436.
[26] S.A. Abdelwahab, Y. Owada, N. Kitanaka, et al., Enhanced expression of adipocyte-type fatty acid binding protein in murine lymphocytes in response to dexamethasone treatment, Mol. Cell Biochem. (2006).
[27] M. Maurer, B. Echtenacher, L. Hultner, et al., The c-kit ligand, stem cell factor, can enhance innate immunity through effects on mast cells, J. Exp. Med. 188 (1998) 2343–2348.
[28] P.C. Calder, Dietary modification of inflammation with lipids, Proc. Nutr. Soc. 61 (2002) 345–358.
[29] L. Makowski, J.B. Boord, K. Maeda, et al., Lack of macrophage fatty-acid-binding protein aP2 protects mice deficient in apolipoprotein E against atherosclerosis, Nat. Med. 7 (2001) 699–705.
[30] S.A. Abdelwahab, Y. Owada, N. Kitanaka, H. Iwasa, H. Sakagami, H. Kondo, Localization of brain-type fatty acid-binding protein in Kupffer cells of mice and its transient decrease in response to lipopolysaccharide, Histochem. Cell Biol. 119 (2003) 469–475.
[31] C. Schachtrup, T.E. Scholzen, V. Grau, et al., L-FABP is exclusively expressed in alveolar macrophages within the myeloid lineage: evidence for a PPARalpha-independent expression, Int. J. Biochem. Cell Biol. 36 (2004) 2042–2053.
[32] M.S. Rolph, T.R. Young, B.O. Shum, et al., Regulation of dendritic cell function and T cell priming by the fatty acid-binding protein AP2, J. Immunol. 177 (2006) 7794–7801.
[33] T. Hanhoff, C. Lucke, F. Spener, Insights into binding of fatty acids by fatty acid binding proteins, Mol. Cell Biochem. 239 (2002) 45–54.
[34] G. Gomez, C. Gonzalez-Espinosa, S. Odom, et al., Impaired FcepsilonRI-dependent gene expression and defective eicosanoid and cytokine production as a consequence of Fyn deficiency in mast cells, J. Immunol. 175 (2005) 7602–7610.
[35] L. Makowski, K.C. Brittingham, J.M. Reynolds, J. Suttles, G.S. Hotamisligil, The fatty acid-binding protein, aP2, coordinates macrophage cholesterol trafficking and inflammatory activity. Macrophage expression of aP2 impacts peroxisome proliferator-activated receptor gamma and IkappaB kinase activities, J. Biol. Chem. 280 (2005) 12888–12895.
[36] N.S. Tan, N.S. Shaw, N. Vinckenbosch, et al., Selective cooperation between fatty acid binding proteins and peroxisome proliferator-activated receptors in regulating transcription, Mol. Cell Biol. 22 (2002) 5114–5127.
[37] H. Qiao, M.V. Andrade, F.A. Lisboa, K. Morgan, M.A. Beaven, FcepsilonR1 and toll-like receptors mediate synergistic signals to markedly augment production of inflammatory cytokines in murine mast cells, Blood 107 (2006) 610–618.
[38] I. Kaneko, T. Hishinuma, K. Suzuki, et al., Prostaglandin F(2alpha) regulates cytokine responses of mast cells through the receptors for prostaglandin E, Biochem. Biophys. Res. Commun. 367 (2008) 590–596.
[39] H. Harizi, N. Gualde, The impact of eicosanoids on the crosstalk between innate and adaptive immunity: the key roles of dendritic cells, Tissue Antigens 65 (2005) 507–514.
[40] S.A. Khan, J.P. Vanden Heuvel, Role of nuclear receptors in the regulation of gene expression by dietary fatty acids (review), J. Nutr. Biochem. 14 (2003) 554–567.